Kinetic sculpting of the seven stripes of the *Drosophila even-skipped* gene

Augusto Berrocal[1,*], Nicholas Lammers[2,*], Hernan G. Garcia[1,2,3,4,$] and Michael B. Eisen[1,2,4,5,6,$]

1. Department of Molecular & Cell Biology, University of California at Berkeley, Berkeley, California
2. Biophysics Graduate Group, University of California at Berkeley, Berkeley, California
3. Department of Physics, University of California at Berkeley, Berkeley, California
4. Institute for Quantitative Biosciences-QB3, University of California at Berkeley, Berkeley, California
5. Department of Integrative Biology, University of California at Berkeley, Berkeley, California
6. Howard Hughes Medical Institute

* co-first authors
$ joint senior authors

Direct correspondence to: mbeisen@berkeley.edu

Abstract

We used live imaging to visualize the transcriptional dynamics of the *Drosophila melanogaster even-skipped* gene at single-cell and high temporal resolution as its iconic seven stripe expression pattern forms. We developed a rigorous quantitative framework for analyzing and visualizing these data, that allows us to infer the temporal dynamics of the transcriptional state of roughly 3,000 nuclei, and characterize how the process varies over time and space. We show that despite being created by the largely independent activity of five discrete enhancers, the seven *eve* stripes are sculpted by the same basic kinetic phenomena: the suppression of bursting outside of stripes, a coupled increase of burst frequency and burst duration within stripes over time and across stripes from their margins to their centers, and the exchange of active nuclei from the posterior to anterior flanks to reposition stripes over time.

Introduction

The patterns of gene expression that choreograph animal development are formed dynamically by an interplay between processes - transcription, mRNA decay and degradation, diffusion, directional transport and the migration of cells and tissues - that vary in both space and time. However the spatial aspects of transcription have dominated the study of developmental gene expression, with the role of temporal processes in shaping patterns receiving comparably little attention (Bothma & Levine 2013).

Gene expression patterns are dynamic on many levels. They form, change and disappear over time, often as cells, tissues and organs are forming and moving in the developing embryo (Lawrence 1992). Furthermore the transcriptional process that creates these patterns is itself highly dynamic. The classical view of transcription as a switch or a tunable rheostat has been replaced in recent years by a picture in which mRNA synthesis occurs in bursts, with promoters switching stochastically between an ON state where polymerases are loaded and begin elongating, and an OFF state where few or no new transcripts are initiated (Figure 1A) (Zenklusen et al. 2008; Golding et al. 2005; Blake et al. 2006; Janicki et al. 2004; Chubb et al. 2006).

A slew of studies, from theoretical models (Ko 1991; Peccoud & Ycart 1995) to imaging-based analyses (Xu et al. 2015; Fukaya et al. 2016; Senecal et al. 2014; Jones et al. 2014), have shown that overall rates of mRNA synthesis can be adjusted by controlling the details of the bursting process. Transcriptional output can be altered by changing the frequency with which bursts occur, their duration, and the rate at which polymerases are loaded during a burst (traditionally specified by k_{on}, k_{off} and r, respectively; Figure 1A). Modulating any or all of these parameters over space and time could in principle produce arbitrarily complex output patterns. However, it remains unclear how diverse the kinetic strategies employed by different regulatory sequences actually are, and what, if anything, constrains how these different kinetic parameters are used by evolution to shape patterns of expression.

In this paper we set out to compare the ways that different enhancers that drive similar types of spatiotemporal patterns during animal development deploy transcriptional bursting to produce their outputs. We use as our model the *Drosophila melanogaster even-skipped* (*eve*) gene whose seven stripes ring the embryo in the cellularizing blastoderm (nuclear cycle 14; nc14) in the hour preceding gastrulation.

The *even-skipped* phenotype was originally described in a screen for mutants that alter the segmented pattern of *D. melanogaster* larvae (Nüsslein-Volhard & Wieschaus 1980), and named based on the absence of the 2nd, 4th, 6th and 8th abdominal segments. Without *eve* activity, segmentation is abolished (Nüsslein-Volhard et al. 1985). Early imaging studies described *eve* as being expressed broadly in nc13 and early nc14 embryos before refining sequentially into four, then seven stripes (Macdonald et al. 1986; Frasch & Levine 1987). Further details of *eve* expression have been uncovered with improved labeling and imaging techniques (Surkova et al. 2008; Fowlkes et al. 2008), which revealed an initial phase with broad domains in the anterior and posterior, followed by the formation of stripes from within these broad domains and, eventually, amplification of the stripe pattern.

The *eve* stripes are produced through the largely independent activity of five discrete enhancers (Figure 1B) that drive individual stripes (the stripe 1, stripe 2, and stripe 5 enhancers) or pairs of stripes (the stripe 3/7 and stripe 4/6 enhancers) (Harding et al. 1989; Goto et al. 1989; Small et al. 1991). These enhancers respond in different ways to canonical maternal factors Bicoid (Bcd) and Caudal (Cad), and gap genes Hunchback (Hb), Giant (Gt), Krüppel (Kr), Knirps (Kni) and Sloppy Paired 1 (Slp1), balancing activating and repressive inputs to generate novel output patterns. For example, the *eve* stripe 2 enhancer is activated in the anterior by Bcd and Hb, and repressed by Gt and Kr, ultimately expressing in a stripe of nuclei that fall between the domains occupied by these two repressors.

The dynamic nature of *eve* stripe formation was highlighted by recent work using live imaging to directly visualize and quantify transcription from an *eve* stripe 2 transgene (Bothma et al. 2014), revealing that the single stripe driven by this enhancer formed and dissipated rapidly, and, significantly, that it was generated by bursts of transcriptional activity in the nuclei that form the stripe.

To do this they utilized the MS2 system, which exploits the interaction between the phage MS2 coat protein (MCP) and a short RNA stem loop to fluorescently label nascent transcripts as they are being synthesized (Bertrand et al. 1998; Garcia et al. 2013; Forrest & Gavis 2003), making it possible to quantify transcription at the single cell level in living embryos. This has led to a series of experimental and theoretical studies of transcriptional bursting in *Drosophila* (Little et al. 2013; Xu et al. 2015; Bothma et al. 2014; Fukaya et al. 2016; Boettiger & Levine 2013; Holloway & Spirov 2017; Zoller et al. 2017) and other systems (Senecal et al. 2014; Golding et al. 2005; Corrigan et al. 2016; Zenklusen et al. 2008).

In this paper we apply the MS2 system to directly visualize and quantify transcription from the intact *eve* locus as the seven stripes form, revealing how a complex pattern of gene expression driven by multiple enhancers is built in space and time at the single cell level.

Our objective in carrying out this work was twofold: first, to characterize the detailed dynamics of this classical and well-studied pattern, and, second to establish a rigorous systematic framework for analyzing such data, and conceptual paradigms for characterizing what we observe from this new type of experiment. Indeed, the advent of live imaging in the context of development calls for the establishment of a new language and new metrics for characterizing the formation of gene expression patterns in space and time.

We use a variety of new computational tools to generate a kinetic fingerprint of *eve* transcription during stripe formation - a record of temporal and spatial variation in the bursting state of the promoters of 3,000 nuclei covering all seven stripes throughout nc14 - and to visualize different aspects of *eve* regulation. We find that all seven *eve* stripes are sculpted by the same regulatory strategies: the elimination of new bursts in “transcriptional deserts” between stripes; the enhancement of bursting over time and across stripes through a coupled increase in k_{on} and decrease in k_{off} ; and the refinement of stripe positions by the addition of bursting nuclei along the anterior edge and the loss of bursting along the posterior edge. Thus, in this experiment and with our new set of analytical tools, we capture not only how single cell transcriptional activity encodes the formation of the stripes, but also how this activity is modulated in time in order to create and displace a complex pattern of gene activity across the embryo.

Results

Live imaging of *eve* expression

We used recombineering (Warming et al. 2005) to modify a bacterial artificial chromosome (BAC) (Venken et al. 2006) containing the *D. melanogaster eve* gene and all of its enhancers and regulatory elements (Venken et al. 2009), replacing the coding region with an array of MS2 stem loops followed by the *D. melanogaster yellow* (*y*) gene (Figure 1C). The 4,329 base pair *y* gene, which is longer than the endogenous *eve* transcript, is phenotypically neutral and provides a means to increase the number of Pol II molecules loaded onto the gene in order to amplify the signal. We inserted the engineered BAC into a targeted site on chromosome 3L

using ΦC31 integrase-mediated recombination (Fish et al. 2007), and homozygosed the line, which showed no signs of adverse effects of the transgene.

We crossed males from this line with females carrying a transgene that expresses in embryos an RFP labeled histone to visualize nuclei, and an MCP-GFP fusion that binds the MS2 RNA stem loops. The result is the direct visualization and quantification of nascent transcripts at the transgene locus as fluorescent puncta (Garcia et al. 2013). The temporal and spatial pattern of *eve* transgene transcription recapitulates the well-characterized dynamics of *eve* expression, most notably formation of the characteristic seven stripes in the late blastoderm (Figure 2; Video 1).

We used laser-scanning confocal microscopy to record, with high temporal resolution and high magnification, two color (MCP-GFP and histone RFP) movies of embryos from before nc14 through gastrulation at the end of nc14. We optimized our data collection strategy to sample multiple stripes (three to five) in each movie, to obtain high temporal resolution (one Z-stack every 16.8 seconds) and to have optimal signal to noise with minimal bleaching. In total, we collected 11 movies (Videos 2-12, available at http://eisenlab.org/eve7), with every stripe imaged at least five times (range 5-9; see Table 1).

We used a custom image processing pipeline (Bothma et al. 2014; Lammers et al. 2018) to identify nuclei, track fluorescent puncta and extract fluorescence intensities in each nucleus over time. The resulting data (File S1) contains fluorescence traces from 2,961 nuclei at an interpolated time interval of 20s, representative examples of which are shown in Figure 3A.

We first sought to reexamine the previously characterized temporal dynamics of stripe formation (Surkova et al. 2008) using the increased temporal resolution (relative to earlier analyses of fixed embryos) of these data (Figure 3B). During nc14, we first observe *eve* transcription beginning approximately five minutes after the onset of anaphase. The initial transcription covers a broad swath of the embryo, from around 25% to 75% egg-length, with the highest activity in two domains roughly centered in the anterior and posterior halves of the embryo respectively. The greatest fluorescence signal during the first 25 minutes of nc14, when stripes are not yet fully formed, is in the most anterior region of *eve* transcription, in an area in which stripe 1 will eventually form.

Although the full seven stripe pattern is not fully formed until around 25 minutes, the three anterior-most stripes are already apparent as locally high areas of fluorescence intensity as early as 10 minutes. By 20 minutes stripes 1,2 and 3 have clearly separated from background, stripes 4 and 6 appear to split off from a large posterior domain, and stripe 7 forms *de novo* in

the posterior. Stripe 5 appears as a distinct strips last, emerging in an area of low transcriptional activity left behind following the splitting of stripes 4 and 6. The stripes persist for the 30 remaining minutes of nc14, gradually increasing in fluorescence intensity until they reach a peak at around 35 minutes into nc14.

The positions of stripes 1-3 along the AP axis are largely stable after they form, while stripes 4-6 show small anterior shifts. Stripe 7 makes a more dramatic movement towards the anterior, moving approximately 8% of egg-length, or around 40 um from its initial location, which is accompanied by a shift in the nuclei driving stripe expression (Figure 3C). This stripe movement, and the decoupling between stripes and nuclei, necessitated the development of a method, described below, to dynamically define the position of stripes throughout each movie.

Modeling and inference of promoter state

As expected, the fluorescence traces from individual nuclei show clear hallmarks of transcriptional bursting, with apparent stochastic fluctuations between states with low and high fluorescence output (Figure 3A). Following previous work in the field, we model bursting as a simple Markovian process in which a promoter switches stochastically between an OFF and an ON state with rates k_{on} and k_{off} in discrete time steps of 20s corresponding to the sampling interval of our data. When the promoter is in the ON state, we assume it loads polymerases continuously throughout the 20s time interval with a constant rate r (Figure 1A).

In our implementation of the MS2 system, once a polymerase molecule transcribes the stem loops located at the 5' end of the gene, the MCP-GFP molecules bound to the stem loops produce a near constant fluorescent signal at the locus that persists until this polymerase completes its traversal of the gene. We determined this polymerase transit time as the displacement that gives the minimum value in autocorrelation of the differences in adjacent time points, with the rationale that every increase in signal due to polymerase loading should be accompanied by a decrease in signal due to the completion of an elongation cycle with a delay equal to the elongation time, arriving at an estimate of 140 seconds (Figure 4A), consistent with a direct measurement of the rate of polymerase elongation of ~2,700 bp/min from (Fukaya et al. 2017) and the length of the construct (6,563bp).

Thus a promoter that is in the ON state at time t loads t x r polymerases and produces a single pulse of fluorescence proportional to t x r (with the proportionality factor determined by the fluorescence of GFP and the fraction of MS2 loops bound by MCP-GFP) that lasts for 140 seconds (Figure 4B). Since we do did not calibrate the fluorescence signal to the number of

polymerase molecules for this construct, in practice we fold the proportionality factor into *r* altering its units from polymerases loaded per unit time to fluorescence signal produced per unit time.

In the embryos we imaged here, the MS2 BAC is heterozygous, contributed only by the father, while the mother contributes the MCP-GFP. However DNA replication occurs within and average of 10 mins for loci in nc14 (McKnight & Miller 1977), meaning that there are actually two sister chromatids with the MS2 containing transgene in every nucleus. And because of sister chromatid cohesion we can not, in general, discriminate both copies. As it is still unclear how the sister chromatids influence each other's transcription, we model the locus as having two independent promoters that operate independently but governed by the same bursting parameters. Thus the system can be in one of three states: OFF, one promoter ON, and two promoters ON.

If we know the state of the promoter over time, we can trivially reconstruct its expected fluorescence output by summing 140s pulses beginning at each point where the promoter is ON and having height *r* if one promoter is ON or height *2* x *r* if two promoters are ON (Figure 4C).

These modeled traces have the features of the observed fluorescence signal: linear increases in intensity (corresponding to periods when the promoter is ON); plateaus (corresponding to periods when transcriptional initiation is matched with previously initiated polymerases completing their transit of the gene); and linear signal decays (corresponding to periods when the promoter is OFF but previously initiated polymerases are still transiting the gene) (Bothma et al. 2014).

However, when given a fluorescence trace, it is not trivial to infer the promoter state sequence that generated it, owing to the time convolution between promoter state and fluorescence output. To solve this problem, we developed a memory-adjusted hidden Markov model (mHMM, described in (Lammers et al. 2018)) that estimates k_{on}, k_{off}, and r. We then fit the model with these parameters to individual traces, inferring the promoter state sequence that optimally reconstructs the fluorescence data from each nucleus.

File S1 contains the inferred promoter state for each nucleus at every time point and the corresponding modeled fluorescence intensity, representative examples of which are shown in Figure 4D-F.

The mHMM accomplishes two aims central to treating these data in a more rigorous and biologically meaningful manner. It allows us to describe the bursting behavior of any set of nuclei in quantitative terms, and, crucially, by providing a means to fit a sequence of ON and

OFF states to the data from each nucleus, the mHMM also allows us to shift the focus in the analysis of individual traces from fluorescence, which only indirectly reflects the temporal behavior of a promoter, to the instantaneous promoter state.

Dynamic determination of stripe positions

Before analyzing the data further we had to solve two practical problems. To compare the kinetic behavior of individual stripes, we had to determine which nuclei were in each stripe at every time point, a process complicated by the movement of stripes relative to both the embryo and nuclei (Figure 3C). And to analyze the data *in toto*, we also had to register the 11 movies relative to each other and to the embryo.

To address these challenges, we used a Gaussian mixture model to cluster bursting nuclei in each movie in a series of overlapping six minute time windows based on their x and y position in the image (Figure 5A). This clustering reliably separates nuclei into individual stripes. We next determined the orientation of each stripe to the AP and imaging axes by fitting a line to coordinates of all nuclei assigned to that stripe in each movie (Figure 5B). We fit a line with this slope to bursting nuclei from each time window (Figures 5C and 5D), and use these fits to generate a linear model of the position of each stripe in each image over time, which we use to reorient the stripe so that it is perpendicular to the image x axis (Figure 5E).

We next use the known coordinates of the anterior and posterior poles of the embryo to convert the image x axis to AP position, and register the examples of each stripe from different movies by setting the AP position of the center of each stripe at 35 mins in nc14 to mean AP position of all examples of that stripe at 35 mins, adjusting the position of the stripe at other time points by the same correction (Figure 5F). As the stripes are not all present until after 25 mins in nc14, we assign and register nuclei before that point based on the stripe position at 25 mins.

A kinetic fingerprint of *eve* stripe formation

Collectively these data represent an easy to visualize and interpret kinetic fingerprint of stripe formation: a record of every transcriptional burst that occurred during the formation of *eve* stripes in these embryos (Figure 6; Video 24).

Eve stripes: transcriptional oases in bursting deserts

We used the output of the mHMM and registration process to examine the locations of transcriptional bursts along the AP axis and over time (Figure 7A). The most striking feature is the almost complete lack of observable transcriptional bursts in the regions between stripes from 25 minutes into nc14, with the exception of the 5-6 interstripe which is discussed below. (Note that this is not an artifact of the movie alignment and orientation process, as these deserts are clearly visible in individual movies.)

These bursting deserts have several evident features. Their spatial boundaries are sharp, with the transition between the low bursting (quiescent) state and the frequently bursting (active) state occurring from one column of nuclei to the next, consistent with the classical descriptions of *eve* stripe patterns (Small et al. 1991). They also have sharp temporal boundaries: all of the bursting deserts, save that between stripes 6 and 7, form in regions where there was appreciable bursting early in nc14 that disappears at around 25 minutes into nc14 (Figure 7A,B)

To better understand how these transcriptional deserts form, we looked at the bursting history of the nuclei in these regions. The first thing we noticed was that, despite the initial period of activity, we do not detect any bursts for a large fraction of nuclei in interstripes at any point during nc14 (Figure 7C). With the exception of the 5-6 interstripe, these never-ON nuclei effectively form the boundaries between stripes, as essentially every nucleus within each stripe bursts at some point during nc14 (Figure 7C,D). The large number of never-ON nuclei is not simply due to a shorter period during which bursts occur, as again with the exception of the 5-6 interstripe, there is already a large difference in the number of nuclei that have burst in stripes compared to interstripes by 15 minutes into nc14 (Figure 7D), before interstripe bursting dissipates.

Despite the large number of never-ON nuclei in interstripes, a significant number of nuclei that ultimately end up in transcriptional deserts do burst in the first 25 minutes of nc14, but become quiescent after this time (Figure 7E, blue nuclei, and 7F). The number of such nuclei increases along the AP axis (Figure 7D), from around 10% of nuclei in the 1-2 interstripe in the anterior to 70% in the 5-6 interstripe in the posterior. Indeed this variation in the number of interstripe nuclei that burst in the first 25 minutes is one of the most striking differences between the different stripes.

Thus, although the specific mechanisms by which these transcriptional deserts are created can vary, the construction of large domains of negligible or reduced bursting is a unified regulatory strategy used to sculpt stripes from regions of initially broad transcription. In our analyses these transcriptional deserts manifest as regions of zero or low k_{on} (Figure 7F),

although with so few observable bursts it is impossible for us to determine if they also represent regions with increased k_{off}. ,

Eve stripes are amplified by a coordinated increase in k_{on} and decrease in k_{off}

Given the reduction of k_{on} over time outside of stripes, we were next interested in examining whether bursting parameters varied within stripes over space and time. To do this, we used the assignment of nuclei to stripes discussed above, and directly estimated bursting parameters within each stripe and its anterior and posterior margins over time using the mHMM-inferred promoter states (Figure 8).

Within stripes, the average fluorescence (Figure 8A) and fraction of nuclei in the ON state (Figure 8B) peak at around 35 min into nc14. This is a product both of a gradual increase in k_{on} in stripe nuclei over time (Figures 8D; see also Figure 7F). This increase in k_{on} is accompanied by a decrease in k_{off} within stripes (Figure 8E) and a corresponding increase in average burst length (Figure 8F).

Figure 8F shows that there is also a decrease in burst length (and thus an increase in k_{off}) in the stripe flanks, suggesting there might be spatial as well as temporal trends in bursting within stripes. To get better spatial resolution, we inferred k_{on} and k_{off} on a nucleus-by-nucleus level during periods of active bursting, and plotted these values against the average AP position of the nucleus (Figure 9A,B). Both k_{on} and k_{off} show strong spatial patterns, with k_{on} highest in the stripe center and decrease towards the stripe flanks, and k_{off} manifesting the opposite trend. We obtained a similar result when we reran the mHMM on subsets of nuclei binned by their stripe position (anterior flank, center and posterior flank; Figure 9C).

The extent to which variation in mean k_{on} and k_{off} appeared coupled led us to examine their relationship in individual nuclei (Figure 10A), which showed a strong inverse correlation of k_{on} and k_{off}. We note that this is not predicted by the stochastic bursting model presented in Figure 1A, which postulates independent k_{on} and k_{off}. To investigate whether this result is an artifact of the mHMM, we implemented an orthogonal method that uses integer programming to infer promoter states from traces based on a direct fit of 140s fluorescence pulses. Crucially this method makes no assumptions about k_{on} and k_{off}, and recapitulates the finding of the correlation between k_{on} and k_{off}. We therefore believe this result is a feature of the data, and not of the method used to model it.

In principle, varying either k_{on} and k_{off}.could independently modulate the transcriptional output of a nucleus with no effect on the other. However across all seven *eve* stripes nuclei that

are more transcriptionally active have both a higher k_{on} and lower k_{off} (Figure 10B). An inverse coupling between k_{on} and k_{off} has been inferred from FISH data (Zoller et al. 2017), but has not been directly measured previously. The ubiquity of this relationship across time and space points highlights the commonality of construction of stripes driven by different enhancers, and, we believe, has important mechanistic implications that we discuss below.

Stripe movement is associated with the dynamic switch of nuclei between active and quiescent states

Previous studies have described the anterior shift of the more posterior *eve* stripes during nc14 (Keränen et al. 2006). This shift has been proposed to arise from a combination of nuclear movement (nuclear flow) and movement in the pattern of regulators (expression flow), especially repressors, which are known to shift anteriorly during nc14 as well (Jaeger, Surkova, et al. 2004; Jaeger, Blagov, et al. 2004). We were interested in whether our ability to track nuclei and their bursting behavior over time might refine our understanding of this process.

We began by examining the nuclei in stripe 7, which, as discussed above, undergoes a dramatic movement of approximately 5 percent of embryo length in the final 25 minutes of nc14. Figure 11A shows the AP positions of the nuclei in one movie covering stripe 7 as a function of time, with the period in which they are part of the stripe highlighted.

Although the stripe is clearly present throughout this period, no nuclei remain a part of the stripe for the entirety of this 25 minute period. As time progresses, nuclei at the posterior edge of stripe 7 shift from an active state, in which the promoter stochastically alternates between the ON and OFF state, to a quiescent state in which we observe no subsequent bursting. In contrast, nuclei just off the anterior edge of the stripe switch from a quiescent to an active state at roughly the same rate. This leads to a net overall anterior movement of the stripe, akin to treadmilling, at a velocity of approximately one percent of embryo length every three minutes.

The other stripes exhibit smaller and varied anterior shifts (Figure 11-S1), but in every case the shift is associated with a similar coupled gain of active nuclei along the anterior edge and loss along the posterior edge. This effect is most clearly seen in Figure 11B, which shows, for each time point where a nucleus initiates a new burst, the difference in activity (defined as the fraction of the time the nucleus is in the ON state in the subsequent 10 min compared to the preceding 10 min). High (red) values represent nuclei that are increasing in activity while low (blue) values represent nuclei decreasing in activity. For all seven stripes there is a clear spatial pattern, with red nuclei along the anterior edge of the stripe and blue nuclei along the posterior

edge, indicating a movement of stripes relative to nuclei, with new nuclei being added at the anterior edge while nuclei are dropped at the posterior edge of the stripe.

Thus, while we see some evidence for the modulation of k_{off} and r, the regulation of burst initiation - k_{on} - is the primary force in sculpting *eve* stripes. Reducing k_{on} is used to create the large areas of limited transcription that define the broad shape of the *eve* pattern; increasing k_{on} is used to boost mRNA production within stripes. And the spatially coordinated switching from low to high k_{on} states is used to reposition stripes along the AP axis. It is these three different manifestations of the regulation of the initiation of transcriptional bursts working together that create the complex and dynamic spatiotemporal gene expression pattern that is *even-skipped*.

Discussion

A stripe is a stripe is a stripe is a stripe is a stripe is a stripe is a stripe

The most remarkable aspect of *eve* regulation is that what appears to be a regular, repeating pattern of nearly identical stripes is created by the largely independent activity of five separate enhancers responding to different combinations of activators and repressors (Fujioka et al. 1999; Fujioka et al. 1995; Small et al. 1991; Arnosti et al. 1996; Small et al. 1992). Our analysis of the time-dependent bursting behavior of nuclei across the embryo reveals that, despite this uniqueness of molecular inputs to each stripe, they employ the same basic regulatory strategy for creating a stripe of transcriptionally active nuclei.

All seven stripes are sculpted by flanking regions of concentrated bursting activity with transcriptional deserts, consisting of a mix of nuclei that never burst during nc14 and nuclei whose bursting is suppressed after stripe formation. All seven stripes add nuclei on their anterior flank and lose nuclei on their posterior flank, although the extent to which this results in stripe movement varies. And from 25 mins into nc14 when the stripes are fully formed, their kinetic fingerprints are highly similar, with increasing k_{on} and decreasing k_{off} across time and across the stripe, no matter which enhancer is driving their expression, no matter which activator they are responding to and no matter which repressor is shaping their boundaries.

The similar bursting profiles of stripes along the AP axis is particularly interesting given that at least four repressors - Gt, Kr, Kni, Hb - and potentially other proteins are involved in forming these boundaries (Clyde et al. 2003). These proteins are known as “short-range” repressors because they act locally, on the scale of at most a few hundred base pairs, to affect the binding and activating capacity of transcriptional activators (Kulkarni & Arnosti 2005; Li & Arnosti 2011;

Payankaulam & Arnosti 2009) - a functional necessity for a gene where one *eve* enhancer can be active in the same nucleus that another nearby enhancer is being repressed. Our data suggest either that there is a common mechanism for short-range repression, perhaps disrupting enhancer:promoter contacts (Chen et al. 2017) or that some selective pressure has tuned enhancers to produce convergent bursting profiles despite differences in repressor activity.

The 5-6 interstripe is also interestesting in this regard, as it has both the highest activity in the first 25 minutes and the highest rate of interstripe bursting after 25 minutes. Expression in the 5-6 interstripe is repressed by Kni acting on the stripe 4-6 enhancer (Clyde et al. 2003) and Gt acting on the stripe 5 enhancer (Fujioka et al. 1999). Given that the relatively common bursting is not observed in the stripe 4-5 interstripe, as would be expected if it were due to incomplete repression by Kni on the stripe 4-6 enhancers, we hypothesize that the relatively high level of 5-6 interstripe bursting is a result of Gt imperfectly repressing transcription from the stripe 5 enhancer. Alone among stripes we do not see a significant modulation in k_{off} across stripe 5, but additional experiments will be required to determine if these observations are related.

In general, where there are differences between stripes, they manifest early. Stripes 1, 2 and 3 appear first, with clear delineation by around 10 minutes into nc14. Some nuclei burst early in the region between the stripe 1, 2 and 3 anlage, but this activity is almost completely gone by 25 minutes. Within these three stripes there is a clear anterior to posterior gradient in the rate at which k_{on} increases (Figure 7D), perhaps reflecting their different positions along the Bcd morphogen gradient. Stripes 4, 5 and 6 become recognizable later than the more anterior stripes, although it is unclear why this is the case (the factors involved in the activation of these stripes are, remarkably, still unclear). Stripe 7 is unique in that it emerges late from an area in which there was little or no previous bursting.

Before generating these data, we expected to find that the two pairs of stripes driven by common enhancers - 3 and 7, and 4 and 6 - might be more similar to each other than they are to the other five stripes. But we do not find this to be the case. Likewise, we expected to see different bursting behavior due to the different activators that regulate the different stripes, and different repressive mechanisms due to the the multiple gap proteins involved in repression. But we do not see such an effect either.

All in all, this commonality of processes used to sculpt *eve* stripes is one of the most striking finding of this paper, and is an emerging theme of studies of transcriptional kinetics. For

examples, the profile of variation in single molecule FISH data suggests that the gap genes involved in segmenting the *Drosophila* blastoderm along the AP axis have a common mode of regulation (Zoller et al. 2017; Little et al. 2013). Here we observe analogous commonalities in live imaging data for different enhancers within the same gene. Whether this represents a constraint imposed by the features of the *eve* promoter or the *Drosophila* cellular blastoderm, or if it reflects convergence among different enhancers or promoters for a common optimal strategy, remains to be seen.

Bursting kinetics and the mechanisms of transcriptional regulation

Although in principle complex patterns of transcription could be generated by the independent regulation of k_{on}, k_{off} or r, many of the key features of *eve* stripe regulation we observe here involve the modulation of k_{on} and k_{off} in concert.

A wide range of earlier studies have inferred bursting parameters from single-molecule FISH experiments using theoretical models (Little et al. 2013; Senecal et al. 2014; Jones et al. 2014; Zoller et al. 2017; So et al. 2011; Zenklusen et al. 2008; Xu et al. 2015; Xu et al. 2016), from manually analyzed MS2 traces (Golding et al. 2005; Fukaya et al. 2016) or signal correlations (Suter et al. 2011; Coulon & Larson 2016; Desponds et al. 2016). Many have used versions of the two state stochastic model used here (Larson et al. 2013; Bar-Even et al. 2006; Zoller et al. 2017; Holloway & Spirov 2017; Xu et al. 2015).

These studies have generally concluded that the main parameter being regulated is k_{on}, however a recent study using single-molecule FISH data of gap gene expression in the *Drosophila* blastoderm concluded that several features of variation in expression could be best explained by a model in which a single parameter controls expression levels (Zoller et al. 2017). From this observation they suggest the system has a distinct characteristic cycle time defined by $1/(k_{on} + k_{off})$ that acts as a constraint that leads to the intrinsic coupling of k_{on} and k_{off}.

By inferring promoter states directly from MS2 data over time and space across multiple stripes we demonstrate this relationship between k_{on} and k_{off} directly, and show that it is an intrinsic feature of bursting data from multiple enhancers, suggesting it has some generality. The fixed characteristic frequency proposed by (Zoller et al. 2017) could generate this relationship, and indeed we do observe a roughly constant $k_{on} + k_{off}$ across a wide range of transcriptional output.

Although the correlation between k_{on} and k_{off} suggests they are mechanistically linked, perhaps the most straightforward explanation for our observation is that k_{on} and k_{off} are

controlled independently by factors whose spatial distributions are linked. Consider, for example, a plausible model in which k_{on} for nuclei in a stripe is a measure of the concentration of the activator(s) acting on the relevant enhancer while k_{off} is a measure of the concentration of the relevant repressor(s). The cross regulation of gap transcription factors produces domains with sharp boundaries that often correspond with stripe borders (Clyde et al. 2003). The resulting local anti-correlated levels of activators and repressors would lead trivially to an anti-correlated k_{on} and k_{off} without having to invoke any shared molecular mechanism.

However, it is also possible that a fundamental assumption of the stochastic model we are using is wrong: that it is not true that the event that initiates a new transcriptional burst occurs only when the promoter is in the OFF state. Consider instead a process - say the physical interaction of an enhancer loaded with essential transcription machinery components (Bansal et al. 2017) and a promoter - that occurs with a frequency that is independent of whether the promoter is engaged in transcription or not. If this interaction occurs when the promoter is OFF, it turns the promoter ON. If it occurs when the promoter is ON, it extends the duration of the current burst (e.g. by increasing the local supply of transcription components).

If these loading events occur randomly but with an adjustable frequency f_b, changing this f_b would adjust the apparent k_{on}, k_{off} and fluorescence in the correlated way we observe. For example, increasing f_b would increase the measured k_{on} as the rate at which new bursts are initiated while the promoter is in the OFF state is dependent directly on f_b, would decrease the measured k_{off} as the rate at which bursts are extended would increase, and would increase the total output of the promoter.

It is also possible that there is a more proximal effect of the binding and unbinding behavior of transcriptional activators. Single-molecule imaging studies have revealed that the binding on and off rates of transcription factors can be modulated in complex ways by their own concentration and the concentration of other factors (Kamar et al. 2017; Mir et al. 2017) and that this can in turn affect all aspect of transcriptional bursting (Senecal et al. 2014).

Whether any aspect of any of these models is correct, and if so what the details are, will require additional data and mechanistic insights. We raise the issue here because our data supportthe possibility that the underlying model we and others rely on to analyze transcriptional kinetics could be parameterized in a manner that does not reflect the underlying biophysics of the process. And that while this model is computationally useful, we wish to caution against too strict a mechanistic interpretation of its parameters.

Stripe movement is driven primarily by expression flow

Just as gene expression patterns are dynamic in time (Bothma et al. 2014), they are dynamic in space, resulting in the movement of expression domains throughout the embryo during development (Jaeger, Surkova, et al. 2004; Keränen et al. 2006). The anterior movement of *eve* stripes during nc14 has been previously described (Keränen et al. 2006), and proposed to arise from a combination of nuclear movement (nuclear flow) and movement in the pattern of regulators (expression flow), especially repressors, which are known to shift anteriorly during nc14 as well (Jaeger, Surkova, et al. 2004; Jaeger, Blagov, et al. 2004). While Keränen *et al.* (Keränen et al. 2006) concluded that the relative contributions of these two forces were roughly equal, our data suggest that, especially in the posterior, expression flow dominates the anterior shift of the *eve* stripes.

A typical nucleus in stripe 7 moves around one percent of embryo length in the final 25 min of nc14. The stripe, however, moves around five percent of embryo length during that time (see Figure 11A). Because we are tracking both the position and activity of individual nuclei, we can visualize expression flow in action. We see nuclei transition from low activity in the anterior interstripe to high activity in the stripe, from high activity in the stripe to low activity off the posterior flank of *eve* expression, and in some cases both.

This effect is most pronounced for the posterior stripes (Figure 11-S1) but is observed for the more anterior stripes as well, although the magnitude of the shift decreases for more anterior stripes. The difference in the amount of the effect we and Keränen *et al.* attribute to expression flow is likely an effect of differences in the data used. Because we are looking at instantaneous transcription rates while they looked at accumulated mRNA, there is a considerable temporal lag and integration of the transcriptional activity over the life time of *eve* mRNA in their data, which has the effect of underestimating the extent to which the stripes actually move.

We also note that the extent to which nuclear flow by itself would be expected to shift output patterns measured as a function of position in the embryo is unclear, as it would depend on the extent to which the repositioning of regulators drives movement of nuclei (which it is believed to do (Blankenship & Wieschaus 2001)), and the corresponding effect that nuclear movement has on the positioning of regulators, which remains largely unknown.

One open question relates to the temporal relationship between changes in the position of the repressor array that drives stripe position and the transcriptional output of the stripes. Recent advances in the simultaneous monitoring of protein concentration and transcriptional

output in living embryos should help answer this question in the near future (Bothma et al. 2018).

Characterizing dynamics patterns demands dynamics measurements

Although *eve* is arguably the gene expression pattern whose *spatial* regulation is best understood, by tracking its single-cell expression as stripes form during nc14, we have revealed several aspects of its *dynamics*, detailed above, that had not been previously appreciated. The most significant observations, the large number of nuclei that never turn on, the measurements of the rates at which the promoter turns ON and OFF, and the shifts in the activity state of nuclei as the repressor arrays move anteriorly, could only have been made with this kind of real-time, single cell data. Further, our data uncovered a plethora of spatiotemporal features that lead to stripe formation whose regulatory rules and detailed underlying molecular mechanisms are yet to be uncovered.

That gene expression is a fundamentally dynamic process is not new information. However, the tools we have had at our disposal to study gene expression so far have tended to emphasize its static features, down to the language we use to describe the transcriptional output of a gene. In textbooks and the scientific literature, *eve* has a gene expression pattern consisting of seven stripes. But, as some earlier work emphasized(Janssens et al. 2006), and we have directly visualized here, the transcriptional output of *eve*, rather than a single “pattern” is a rapidly changing as a function of time and space: it is dynamic at many time scales and across space and nuclear positions. Indeed, at no point does *eve* approach anything even remotely like a steady state.

We are at the dawn of a new period in the study of transcription, as new experimental techniques and advanced microscopy allow us to monitor transcriptional regulators, observe their behavior at the single-molecule level, and track the transcriptional output of a gene in living, developing animals. We have only barely begun to understand this new data and what it can tell us about biology. While the focus in this paper was on a single gene in a single species, we hope that this and our accompanying work (Lammers et al. 2018) will have a broader impact by beginning to establish rigorous frameworks for quantifying, characterizing and visualizing the dynamics of transcription at the single-cell level during development that will be required in the era of live imaging of transcription in development.

Methods

Generation of MS2 tagged *eve* BAC

We used bacterial recombineering (Warming et al. 2005) to modify a bacterial artificial chromosome (BAC) (Venken et al. 2006) containing the *D. melanogaster eve* gene and all of its enhancers and regulatory elements (BAC CH322-103K22) (Venken et al. 2009), replacing the coding region with an array of 24 MS2 stem loops fused with *D. melanogaster yellow* gene [(Bothma et al. 2014)] (Figure 1B). We inserted our eve::MS2::yellow BAC-based construct in *D.melanogaster* genome at chromosome 3L through ΦC31 integrase-mediated recombination (see Generation of fly lines), and generated a viable homozygous fly line (w-; +; eve::MS2::yellow).

Specifics of recombineering

We modified a CHORI BAC CH322-103K22 derived from (Venken et al. 2009), which contained the entire *eve* locus and a GFP reporter instead of *eve* coding sequence (CH322-103K22-GFP). We replaced the GFP reporter with MS2::*yellow* (6665 bp) through a two step, scarless, *galK* cassette-mediated bacterial recombineering (Warming et al. 2005). Briefly, we transformed our starting CH322-103K22-GFP BAC in *E.coli* recombineering strain SW102. We then electroporated the strain with a *galK* cassette flanked by 50bp-long DNA homology arms homologous to the MS2::*yellow* (6665 bp) reporter. Upon electroporation, we selected transformants on M63 minimal media plates with galactose as a single carbon source. We achieved a correct replacement of GFP sequence by *galK* cassette in the BAC context (CH322-103K22-galK), validated by observing the digestion patterns produced by ApaLI restriction enzyme.

We purified CH322-103K22-galK BAC and transformed it into fresh *E.coli* SW102 cells. Next, we electroporated these cells with the purified MS2::*yellow* insert. We used M63 minimal media plates with 2-deoxy-galactose to select against bacteria with a functional *galK* gene, and used colony PCR to screen for colonies with a correct MS2::*yellow* insertion (CH322-103K22-MS2) replacing the *galK* cassette. We validated this insertion by observing ApaLI, XhoI, SmaI, and EcoRI restriction digestion patterns and through PCR and Sanger sequencing of the insertion junctions. We transformed our CH322-103K22-MS2 BAC in *E.coli* EPI300 cells to induce high copy number and purified it with a Qiagen plasmid Midiprep kit.

Generation of fly lines

We sent a sample of our purified CH322-103K22-MS2 BAC to Rainbow Transgenic Flies, Inc. for injection in *D.melanogaster* embryos bearing a ΦC31 AttP insertion site in chromosome 3L (Bloomington stock #24871; landing site VK00033; cytological location 65B2). We received the flies that resulted from that injection and used a balancer fly line (w- ; + ; +/TM3sb) to obtain a viable MS2 homozygous line (w- ; + ; MS2::*yellow*). We used line (yw; His::RFP; MCP::GFP) as the maternal source of Histone-RFP and MCP-GFP (Garcia et al. 2013).

Embryo Collection and Mounting

Embryo collection and mounting was done as specified in (Garcia & Gregor 2018). In short, we set fly crosses between ~30 males (w-; +; eve::MS2::yellow) and ~80 females (yw; His::RFP; MCP::GFP) in a plastic cage capped with a grape juice agar plate. We collected embryos from cages two to ten days old by adding a fresh plate for 30 minutes and aging for 60 minutes to target embryos 90 min or younger. We embedded a gas-permeable Lumox Film (Sarstedt - Catalog # 94.6077.317) on a microscope slide hollowed on the center. Then, we coated the hydrophobic side of the Lumox film with heptane glue and let it dry. The film allows oxygenation of embryos during the 2-3h long imaging sessions while heptane immobilize them.

We soaked an agar plate with Halocarbon 27 oil, picked embryos with forceps, and laid them down on a 3 x 3 cm piece of paper tissue. We dechorionated embryos by adding 2 drops of bleach diluted in water (5.25%) on the paper tissue and incubating for 1.5 minute. We removed bleach with a clean tissue and rinsed with ~4 drops of distilled water. We then placed the tissue paper with dechorionated embryos in water, and picked buoyant embryos with a brush.

We lined ~30 apparently healthy embryos on the Lumox film slide and added 2-3 drops of Halocarbon 27 oil to avoid desiccation, and covered the embryos with a cover slip (Corning® Cover Glass, No.1, 18 x 18mm) for live imaging.

Imaging and Optimization of Data Collection

Movies of embryonic development were recorded on a Zeiss-800 confocal laser scanning microscope in two channels, (EGFP: 488 nm; TagRFP: 561 nm). We imaged embryos on a wide field of view, along their anterior-posterior axis, of 1024 x 256 pixels (202.8μm x 50.7μm), encompassing 3-5 stripes per movie. We optimized laser power, scanning parameters, master

gain, pinhole size and laser power to optimize signal to noise ratio without significant photobleaching and phototoxicity.

For imaging, the following microscope settings were used: 63X oil-objective, scan mode 'frame', pixel size of 0.2µm, 16 bits per pixel, bidirectional scanning at a speed of 7, line step of 1, laser scanner dwelling per pixel of 1.03µs, laser scanner averaging of 2, averaging method Mean, averaging mode Line, 488 nm laser power of 30µW (EGFP), 561 nm laser power of 7.5µW (TagRFP) (both powers were measured with the 10X air-objective), Master Gain in EGFP detector of 550V, Master Gain in TagRFP detector of 650V, Digital Offset in both detectors of 0, Digital Gain in both detectors of 1.0, and a pinhole size of 1 airy unit under the imaging conditions mentioned above (44µm, 0.7µm/section), laser filters EGFP:SP545 and TagRFP:LBF640. This resulted in an imaging time of 633 ms per frame and a full Z-stack of 21 frames in intervals of 0.5µm every 16.8s. We stopped imaging after 50 min into nuclear cycle 14, and took mid-sagittal and surface pictures of the whole embryo for localization of the recorded field of view along the embryo's AP axis.

Image processing

We used a Matlab computational pipeline based on (Garcia et al. 2013; Lammers et al. 2018) to segment and extract numeric data from our raw movies. Briefly, this software segments and processes the images from the two channels (channel 1: MCP::GFP, channel 2: Histone::RFP) on which we collected our data. For segmentation of channel 1, we used Fiji-Weka Segmentation 3D software; this machine-learning-based method relies on the manual segmentation of a variety of MCP::GFP labeled transcriptional foci in a given 21 frame Z-stack from a single dataset (EVE_D11) to produce a model for the segmentation of all datasets recorded under the same imaging conditions. Next, we segmented and tracked the Histone::RFP labeled nuclei on channel 2. Subsequently, we assigned MCP::GFP labeled transcriptional foci to their corresponding Histone::RFP labeled nuclei. Since we collected whole embryo pictures of each of our datasets, we were able to match and locate the recorded fields of view to their right position along the body of their corresponding embryos. Finally, we extracted position and fluorescence values over time of all transcriptional foci to generate data structures ready to use in further analyses.

Memory-Adjusted Hidden Markov Model

For this work we employed a statistical method that utilizes memory-adjusted Hidden Markov Models to infer bursting parameters from experimental fluorescence traces. The theory and implementation of this method are described in detail in (Lammers et al. 2018). Briefly, parameters were inferred using a standard version of the Expectation Maximization (EM) Algorithm implemented using custom-written scripts in Matlab. Bootstrap sampling was used to estimate the standard error in our parameter estimates. Subsets of 8,000 data points were used to generate time-averaged parameter estimates. Sample sizes for windowed inference varied due to data set limitations. When possible, samples of 4,000 points were used. Inference was not conducted for spatio-temporal regions for which fewer than 1,000 time points were available.

Data Analysis and Figures

All data were analyzed in Python using a Jupyter notebook with custom code to process raw data and generate figures. The Jupyter notebook and all data required to run it is available in File S1.

Data Filtering

We first filtered the raw data to remove data with observations spanning less than 2,000 seconds, as well as nuclei that were poorly tracked over time (defined as nuclei that moved across the movies at an average rate of over 4.5 pixels per minute. This left 430,073 observations from 2,959 nuclei.

Stripe assignment and registration

We used the Gaussian mixture model module of the Python library scikit-learn (Pedregosa et al. 2011) to cluster all nuclei time points in each movie in each of a series of overlapping 428 second time windows beginning at 25 mins in nc14, specifying the number of components equal to the number of stripes captured in the movie and using the setting *covariance_type='tied'.* We preliminarily assigned nuclei time points to a stripe if they were consistently clustered in that stripe in the relevant time windows. We then pooled all nuclei time points assigned to the same stripe and fit a line to the median x and y positions in the bottom ($y < 128$) and top ($y > 128$) halves of the image. We considered the slope of this line to represent the orientation of the stripe to the image x axis. We then went back to each time window and fit the nuclei assigned to the stripe with a line with the previously computed slope fixed. This produced an association of

time with stripe position, from which we derived a linear model that describes the position of each stripe in each movie at every time point.

We assigned all nuclei time points (not just bursting ones) to stripes by identifying the stripe whose predicted position at the relevant time was closest (along the x axis) to the nucleus being analyzed, and assigned a nucleus to the most common stripe assignment for its individual time points. We then corrected the reorientation of the stripe at each time point to be perpendicular to the image x axis (to enable projection along the AP axis) by setting its new image x axis position to be the x position of the stripe in the middle of the y axis (y = 128) plus the offset of the nucleus to the unoriented stripe along the x axis. For some visualizations we further adjusted the position of each nucleus time point to correct for stripe movement.

Finally, we used the positions of the anterior and posterior poles of the embryo to map image x coordinates to AP position. We then adjusted the AP position of each stripe in each movie such that the center of the stripe at 35 mins in nc14 had the same AP position.

Local on and off rate calculations

We computed a “local” on and off rate for individual nuclei or collections of nuclei as follows. The local on rate was defined as the number of timepoints where the promoter transition from OFF to ON divided by total number of timepoints in the OFF state, while the local off rate was defined as number of timepoints where the promoter transition from ON to OFF divided by total number of timepoints in the ON state.

Author contributions

AB designed and generated the labeled *eve* transgene, collected all of the imaging data and ran the initial image processing. NL and MBE performed all of the higher level analyses and generated figures. MBE wrote the paper. HGG and MBE conceived of the experiments. HGG and MBE provided funding and supervised every aspect of the project.

Data Availability

All of the raw and processed data described in this paper as well as links to code and computational notebooks are available in File S1 and at http://www.eisenlab.org/eve7.

Acknowledgements

This work was supported by an HHMI Investigator award to MBE. HGG was supported by the Burroughs Wellcome Fund Career Award at the Scientific Interface, the Sloan Research Foundation, the Human Frontiers Science Program, the Searle Scholars Program, the Shurl & Kay Curci Foundation, the Hellman Foundation, the NIH Director's New Innovator Award (DP2 OD024541-01), and an NSF CAREER Award (1652236). NL was supported by NIH Genomics and Computational Biology training grant 5T32HG000047-18. AB was supported by a University of California Institute for Mexico and the United States (UC MEXUS) - CONACyT Doctoral Fellowship.

Tables

Table 1. Summary of movies collected.

Embryo ID	Duration	Stripes	Data Movies	Promoter State Movies
EVE_D1	255 frames 71.2 min	1-4	Video 2	Video 13
EVE_D2	254 frames 70.9 min	3-7	Video 3	Video 14
EVE_D3	235 frames 65.6 min	3-6	Video 4	Video 15
EVE_D4	246 frames 68.7 min	3-7	Video 5	Video 16
EVE_D5	210 frames 58.6 min	4-7	Video 6	Video 17
EVE_D6	196 frames 54.7 min	4-7	Video 7	Video 18
EVE_D7	208 frames 58.1 min	3-7	Video 8	Video 19
EVE_D8	232 frames 64.8 min	1-3	Video 9	Video 20
EVE_D9	322 frames 89.9 min	1-4	Video 10	Video 21
EVE_D10	267 frames 74.5 min	1-3	Video 11	Video 22
EVE_D11	307 frames 85.7 min	1-4	Video 12	Video 23

All videos are available at http://www.eisenlab.org/eve7/movies. All data videos 16.76 fps. Promoter state movies are at 20 fps.

Videos

Video 1. Full expression pattern of *eve*-MS2 BAC

Maximum value projection of z-stacks of entire embryo carrying *eve*-MS2 BAC, MCP-GFP and histone-RFP imaged with a 40x objective.

Videos 2-12. Individual dataset movies

Maximum value projection of z-stacks of sections of embryos carrying *eve*-MS2 BAC, MCP-GFP and histone-RFP imaged with a 63x objective capturing 3-5 stripes as described in Table 1.

Video 13-23. Promoter state movies

Animation of pseudo-cells (a Voronoi tessellation based on the position of nuclei) where cells are colored based on their stripe, with intensity proportional to the measured fluorescence of the nucleus at the given time, and promoters in the ON state represented with white outlines of the pseudo-cell.

Video 24. Kinetic fingerprint of *eve* stripe formation

Nuclei are graphed at every time point graphed at its AP (x-axis) and image y (y-axis) position when the mHMM inferred that the promoter was in the ON state.

References

Arnosti, D.N. et al., 1996. The eve stripe 2 enhancer employs multiple modes of transcriptional synergy. *Development* , 122(1), pp.205–214.

Bansal, K. et al., 2017. The transcriptional regulator Aire binds to and activates super-enhancers. *Nature immunology*, 18(3), pp.263–273. Available at: http://dx.doi.org/10.1038/ni.3675.

Bar-Even, A. et al., 2006. Noise in protein expression scales with natural protein abundance. *Nature genetics*, 38(6), pp.636–643. Available at: http://dx.doi.org/10.1038/ng1807.

Bertrand, E. et al., 1998. Localization of ASH1 mRNA particles in living yeast. *Molecular cell*, 2(4), pp.437–445. Available at: https://www.ncbi.nlm.nih.gov/pubmed/9809065.

Blake, W.J. et al., 2006. Phenotypic consequences of promoter-mediated transcriptional noise. *Molecular cell*, 24(6), pp.853–865. Available at: http://dx.doi.org/10.1016/j.molcel.2006.11.003.

Blankenship, J.T. & Wieschaus, E., 2001. Two new roles for the Drosophila AP patterning system in early morphogenesis. *Development* , 128(24), pp.5129–5138. Available at: https://www.ncbi.nlm.nih.gov/pubmed/11748148.

Boettiger, A.N. & Levine, M., 2013. Rapid transcription fosters coordinate snail expression in the Drosophila embryo. *Cell reports*, 3(1), pp.8–15. Available at: http://dx.doi.org/10.1016/j.celrep.2012.12.015.

Bothma, J. & Levine, M., 2013. Development: Lights, Camera, Action — The Drosophila Embryo Goes Live! *Current biology: CB*, 23(21), pp.R965–R967. Available at: http://dx.doi.org/10.1016/j.cub.2013.09.054.

Bothma, J.P. et al., 2014. Dynamic regulation of eve stripe 2 expression reveals transcriptional bursts in living Drosophila embryos. *Proceedings of the National Academy of Sciences*, 111(29), pp.10598–10603. Available at: http://www.pnas.org/content/111/29/10598.abstract.

Bothma, J.P. et al., 2018. LlamaTags: A Versatile Tool to Image Transcription Factor Dynamics in Live Embryos. *Cell*, 0(0). Available at: http://www.cell.com.libproxy.berkeley.edu/article/S009286741830401X/abstract [Accessed May 12, 2018].

Chen, H., Fujioka, M. & Gregor, T., 2017. Direct visualization of transcriptional activation by physical enhancer-promoter proximity. *bioRxiv*, p.099523. Available at: https://www.biorxiv.org/content/early/2017/01/11/099523 [Accessed June 9, 2018].

Chubb, J.R. et al., 2006. Transcriptional pulsing of a developmental gene. *Current biology: CB*, 16(10), pp.1018–1025. Available at: http://dx.doi.org/10.1016/j.cub.2006.03.092.

Clyde, D.E. et al., 2003. A self-organizing system of repressor gradients establishes segmental complexity in Drosophila. *Nature*, 426(6968), pp.849–853. Available at:

http://dx.doi.org/10.1038/nature02189.

Corrigan, A.M. et al., 2016. A continuum model of transcriptional bursting. *eLife*, 5, p.e13051. Available at: https://elifesciences.org/articles/13051 [Accessed March 30, 2018].

Coulon, A. & Larson, D.R., 2016. Fluctuation Analysis: Dissecting Transcriptional Kinetics with Signal Theory. *Methods in enzymology*, 572, pp.159–191. Available at: http://dx.doi.org/10.1016/bs.mie.2016.03.017.

Desponds, J. et al., 2016. Precision of Readout at the hunchback Gene: Analyzing Short Transcription Time Traces in Living Fly Embryos. *PLoS computational biology*, 12(12), p.e1005256. Available at: http://journals.plos.org/ploscompbiol/article/file?id=10.1371/journal.pcbi.1005256&type=printable [Accessed May 31, 2018].

Fish, M.P. et al., 2007. Creating transgenic Drosophila by microinjecting the site-specific phiC31 integrase mRNA and a transgene-containing donor plasmid. *Nature protocols*, 2(10), pp.2325–2331. Available at: http://dx.doi.org/10.1038/nprot.2007.328.

Forrest, K.M. & Gavis, E.R., 2003. Live imaging of endogenous RNA reveals a diffusion and entrapment mechanism for nanos mRNA localization in Drosophila. *Current biology: CB*, 13(14), pp.1159–1168. Available at: https://www.ncbi.nlm.nih.gov/pubmed/12867026.

Fowlkes, C.C. et al., 2008. A quantitative spatiotemporal atlas of gene expression in the Drosophila blastoderm. *Cell*, 133(2), pp.364–374. Available at: http://dx.doi.org/10.1016/j.cell.2008.01.053.

Frasch, M. & Levine, M., 1987. Complementary patterns of even-skipped and fushi tarazu expression involve their differential regulation by a common set of segmentation genes in Drosophila. *Genes & development*, 1(9), pp.981–995. Available at: https://www.ncbi.nlm.nih.gov/pubmed/2892761.

Fujioka, M. et al., 1999. Analysis of an even-skipped rescue transgene reveals both composite and discrete neuronal and early blastoderm enhancers, and multi-stripe positioning by gap gene repressor gradients. *Development* , 126(11), pp.2527–2538. Available at: https://www.ncbi.nlm.nih.gov/pubmed/10226011.

Fujioka, M., Jaynes, J.B. & Goto, T., 1995. Early even-skipped stripes act as morphogenetic gradients at the single cell level to establish engrailed expression. *Development* , 121(12), pp.4371–4382. Available at: https://www.ncbi.nlm.nih.gov/pubmed/8575337.

Fukaya, T., Lim, B. & Levine, M., 2016. Enhancer Control of Transcriptional Bursting. *Cell*, 166(2), pp.358–368. Available at: http://dx.doi.org/10.1016/j.cell.2016.05.025.

Fukaya, T., Lim, B. & Levine, M., 2017. Rapid Rates of Pol II Elongation in the Drosophila Embryo. *Current biology: CB*, 27(9), pp.1387–1391. Available at: http://dx.doi.org/10.1016/j.cub.2017.03.069.

Garcia, H.G. et al., 2013. Quantitative imaging of transcription in living Drosophila embryos links polymerase activity to patterning. *Current biology: CB*, 23(21), pp.2140–2145. Available at:

http://dx.doi.org/10.1016/j.cub.2013.08.054.

Garcia, H.G. & Gregor, T., 2018. Live Imaging of mRNA Synthesis in Drosophila. *Methods in molecular biology* , 1649, pp.349–357. Available at: http://dx.doi.org/10.1007/978-1-4939-7213-5_23.

Golding, I. et al., 2005. Real-Time Kinetics of Gene Activity in Individual Bacteria. *Cell*, 123(6), pp.1025–1036. Available at: http://www.cell.com/abstract/S0092-8674(05)01037-8 [Accessed April 12, 2018].

Goto, T., Macdonald, P. & Maniatis, T., 1989. Early and late periodic patterns of even skipped expression are controlled by distinct regulatory elements that respond to different spatial cues. *Cell*, 57(3), pp.413–422. Available at: http://www.cell.com/abstract/0092-8674(89)90916-1 [Accessed May 9, 2018].

Harding, K. et al., 1989. Autoregulatory and gap gene response elements of the even-skipped promoter of Drosophila. *The EMBO journal*, 8(4), pp.1205–1212. Available at: http://www.ncbi.nlm.nih.gov/pubmed/2743979.

Holloway, D.M. & Spirov, A.V., 2017. Transcriptional bursting in Drosophila development: Stochastic dynamics of eve stripe 2 expression. *PloS one*, 12(4), p.e0176228. Available at: http://journals.plos.org/plosone/article/file?id=10.1371/journal.pone.0176228&type=printable [Accessed March 30, 2018].

Jaeger, J., Blagov, M., et al., 2004. Dynamical analysis of regulatory interactions in the gap gene system of Drosophila melanogaster. *Genetics*, 167(4), pp.1721–1737. Available at: http://dx.doi.org/10.1534/genetics.104.027334.

Jaeger, J., Surkova, S., et al., 2004. Dynamic control of positional information in the early Drosophila embryo. *Nature*, 430(6997), pp.368–371. Available at: http://dx.doi.org/10.1038/nature02678.

Janicki, S.M. et al., 2004. From silencing to gene expression: real-time analysis in single cells. *Cell*, 116(5), pp.683–698. Available at: https://www.ncbi.nlm.nih.gov/pubmed/15006351.

Janssens, H. et al., 2006. Quantitative and predictive model of transcriptional control of the Drosophila melanogaster even skipped gene. *Nature genetics*, 38(10), pp.1159–1165. Available at: http://dx.doi.org/10.1038/ng1886.

Jones, D.L., Brewster, R.C. & Phillips, R., 2014. Promoter architecture dictates cell-to-cell variability in gene expression. *Science*, 346(6216), pp.1533–1536. Available at: http://dx.doi.org/10.1126/science.1255301.

Kamar, R.I. et al., 2017. Facilitated dissociation of transcription factors from single DNA binding sites. *Proceedings of the National Academy of Sciences of the United States of America*, 114(16), pp.E3251–E3257. Available at: http://dx.doi.org/10.1073/pnas.1701884114.

Keränen, S.V.E. et al., 2006. Three-dimensional morphology and gene expression in the Drosophila blastoderm at cellular resolution II: dynamics. *Genome biology*, 7(12), p.R124.

Available at: http://dx.doi.org/10.1186/gb-2006-7-12-r124.

Ko, M.S.H., 1991. A stochastic model for gene induction. *Journal of theoretical biology*, 153(2), pp.181–194. Available at: http://www.sciencedirect.com/science/article/pii/S0022519305804217.

Kulkarni, M.M. & Arnosti, D.N., 2005. cis-regulatory logic of short-range transcriptional repression in Drosophila melanogaster. *Molecular and cellular biology*, 25(9), pp.3411–3420. Available at: http://dx.doi.org/10.1128/MCB.25.9.3411-3420.2005.

Lammers, N. et al., 2018. Binary transcriptional control of pattern formation in development. Available at: https://www.biorxiv.org/content/early/2018/05/31/335919.

Larson, D.R. et al., 2013. Direct observation of frequency modulated transcription in single cells using light activation. *eLife*, 2, p.e00750. Available at: https://elifesciences.org/articles/00750 [Accessed June 8, 2018].

Lawrence, P.A., 1992. *The Making of a Fly: The Genetics of Animal Design* 1 edition., Wiley-Blackwell. Available at: https://www.amazon.com/Making-Fly-Genetics-Animal-Design/dp/0632030488.

Li, L.M. & Arnosti, D.N., 2011. Long- and short-range transcriptional repressors induce distinct chromatin states on repressed genes. *Current biology: CB*, 21(5), pp.406–412. Available at: http://dx.doi.org/10.1016/j.cub.2011.01.054.

Little, S.C., Tikhonov, M. & Gregor, T., 2013. Precise Developmental Gene Expression Arises from Globally Stochastic Transcriptional Activity. *Cell*, 154(4), pp.789–800. Available at: http://www.cell.com/abstract/S0092-8674(13)00896-9 [Accessed April 12, 2018].

Macdonald, P.M., Ingham, P. & Struhl, G., 1986. Isolation, structure, and expression of even-skipped: a second pair-rule gene of Drosophila containing a homeo box. *Cell*, 47(5), pp.721–734. Available at: https://www.ncbi.nlm.nih.gov/pubmed/2877745.

McKnight, S.L. & Miller, O.L., Jr, 1977. Electron microscopic analysis of chromatin replication in the cellular blastoderm Drosophila melanogaster embryo. *Cell*, 12(3), pp.795–804. Available at: https://www.ncbi.nlm.nih.gov/pubmed/411576.

Mir, M. et al., 2017. Dense Bicoid hubs accentuate binding along the morphogen gradient. *Genes & development*, 31(17), pp.1784–1794. Available at: http://dx.doi.org/10.1101/gad.305078.117.

Nüsslein-Volhard, C., Kluding, H. & Jürgens, G., 1985. Genes affecting the segmental subdivision of the Drosophila embryo. *Cold Spring Harbor symposia on quantitative biology*, 50, pp.145–154. Available at: https://www.ncbi.nlm.nih.gov/pubmed/3868475.

Nüsslein-Volhard, C. & Wieschaus, E., 1980. Mutations affecting segment number and polarity in Drosophila. *Nature*, 287(5785), pp.795–801. Available at: https://www.ncbi.nlm.nih.gov/pubmed/6776413.

Payankaulam, S. & Arnosti, D.N., 2009. Groucho corepressor functions as a cofactor for the

Knirps short-range transcriptional repressor. *Proceedings of the National Academy of Sciences of the United States of America*, 106(41), pp.17314–17319. Available at: http://dx.doi.org/10.1073/pnas.0904507106.

Peccoud, J. & Ycart, B., 1995. Markovian Modeling of Gene-Product Synthesis. *Theoretical population biology*, 48(2), pp.222–234. Available at: http://www.sciencedirect.com/science/article/pii/S0040580985710271.

Pedregosa, F. et al., 2011. Scikit-learn: Machine Learning in Python. *Journal of machine learning research: JMLR*, 12(Oct), pp.2825–2830. Available at: http://www.jmlr.org/papers/volume12/pedregosa11a/pedregosa11a.pdf [Accessed June 7, 2018].

Senecal, A. et al., 2014. Transcription factors modulate c-Fos transcriptional bursts. *Cell reports*, 8(1), pp.75–83. Available at: http://dx.doi.org/10.1016/j.celrep.2014.05.053.

Small, S. et al., 1991. Transcriptional regulation of a pair-rule stripe in Drosophila. *Genes & development*, 5(5), pp.827–839. Available at: http://www.ncbi.nlm.nih.gov/pubmed/2026328.

Small, S., Blair, A. & Levine, M., 1992. Regulation of even-skipped stripe 2 in the Drosophila embryo. *The EMBO journal*, 11(11), pp.4047–4057. Available at: http://www.ncbi.nlm.nih.gov/pubmed/1327756.

So, L.-H. et al., 2011. General properties of transcriptional time series in Escherichia coli. *Nature genetics*, 43(6), pp.554–560. Available at: http://dx.doi.org/10.1038/ng.821.

Surkova, S. et al., 2008. Characterization of the Drosophila segment determination morphome. *Developmental biology*, 313(2), pp.844–862. Available at: http://dx.doi.org/10.1016/j.ydbio.2007.10.037.

Suter, D.M. et al., 2011. Mammalian Genes Are Transcribed with Widely Different Bursting Kinetics. *Science*, 332(6028), pp.472–474. Available at: http://science.sciencemag.org/content/332/6028/472 [Accessed June 8, 2018].

Venken, K.J.T. et al., 2006. P[acman]: a BAC transgenic platform for targeted insertion of large DNA fragments in D. melanogaster. *Science*, 314(5806), pp.1747–1751. Available at: http://dx.doi.org/10.1126/science.1134426.

Venken, K.J.T. et al., 2009. Versatile P[acman] BAC libraries for transgenesis studies in Drosophila melanogaster. *Nature methods*, 6(6), pp.431–434. Available at: http://dx.doi.org/10.1038/nmeth.1331.

Warming, S. et al., 2005. Simple and highly efficient BAC recombineering using galK selection. *Nucleic acids research*, 33(4), p.e36. Available at: http://dx.doi.org/10.1093/nar/gni035.

Xu, H. et al., 2015. Combining protein and mRNA quantification to decipher transcriptional regulation. *Nature methods*, 12(8), pp.739–742. Available at: http://dx.doi.org/10.1038/nmeth.3446.

Xu, H. et al., 2016. Stochastic Kinetics of Nascent RNA. *Physical review letters*, 117(12). Available at: http://dx.doi.org/10.1103/PhysRevLett.117.128101.

Zenklusen, D., Larson, D.R. & Singer, R.H., 2008. Single-RNA counting reveals alternative modes of gene expression in yeast. *Nature structural & molecular biology*, 15(12), pp.1263–1271. Available at: http://dx.doi.org/10.1038/nsmb.1514.

Zoller, B., Little, S.C. & Gregor, T., 2017. Diverse spatial expression patterns emerge from common transcription bursting kinetics. *arXiv [q-bio.SC]*. Available at: http://arxiv.org/abs/1712.08215.

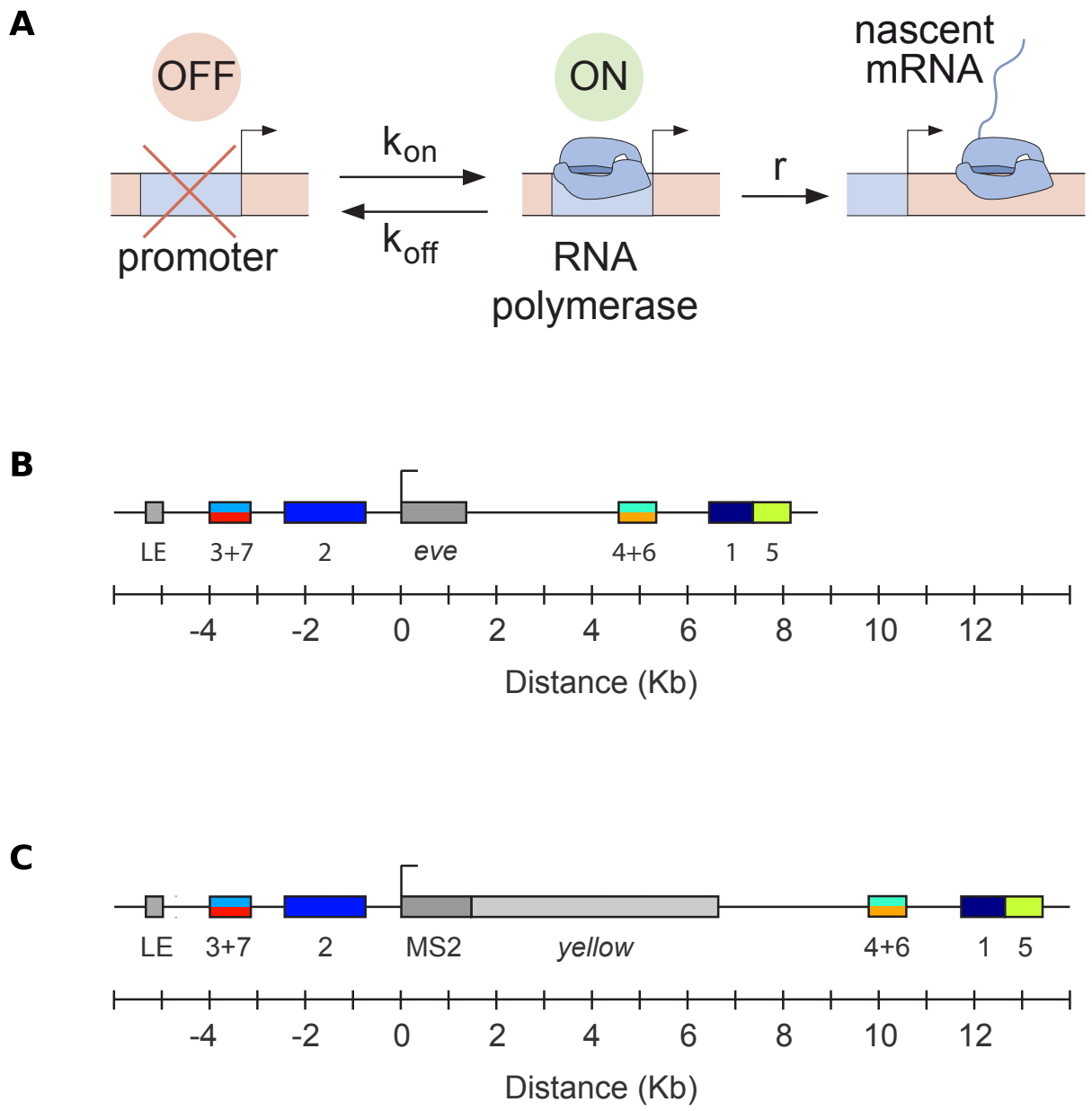

Figure 1. Visualizing live transcription from the seven stripes of D. melanogaster even-skipped.

A) Simple model of transcriptional bursting by promoter switching between ON and OFF states. B) Wild-type eve locus showing the five stripe enhancers (1,2,3+7,4+6,5) and the late enhancer (LE). C) Layout of the engineered eve BAC showing the location of the MS2 array and yellow gene.

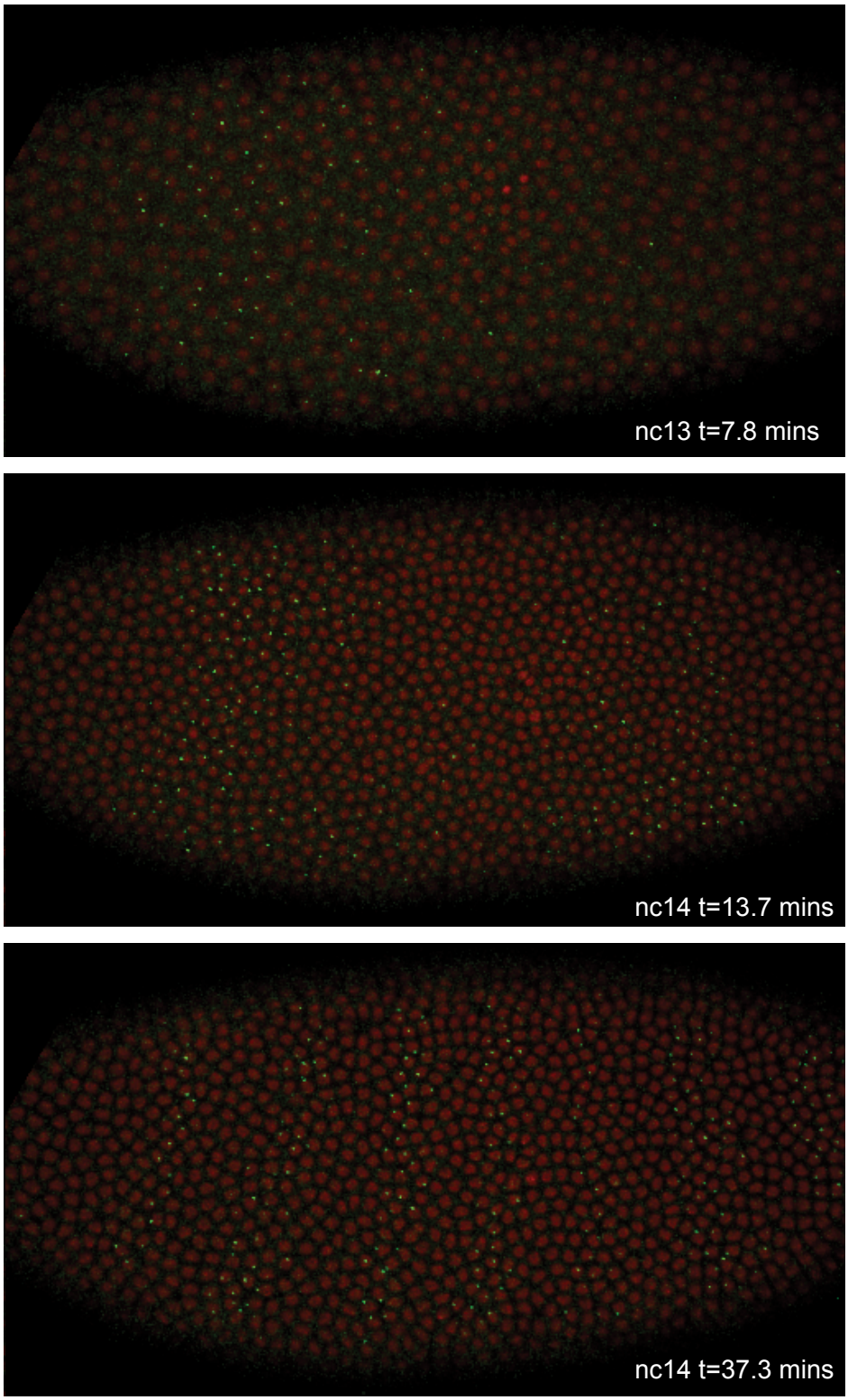

Figure 2. Live expression of even-skipped

Stills from maximum projection renderings of image stacks of an embryo spanning all seven stripes. This movie was collected at 40x resolution for illustration purposes only. Movies used for data analysis were collected at higher resolution as described in the text.

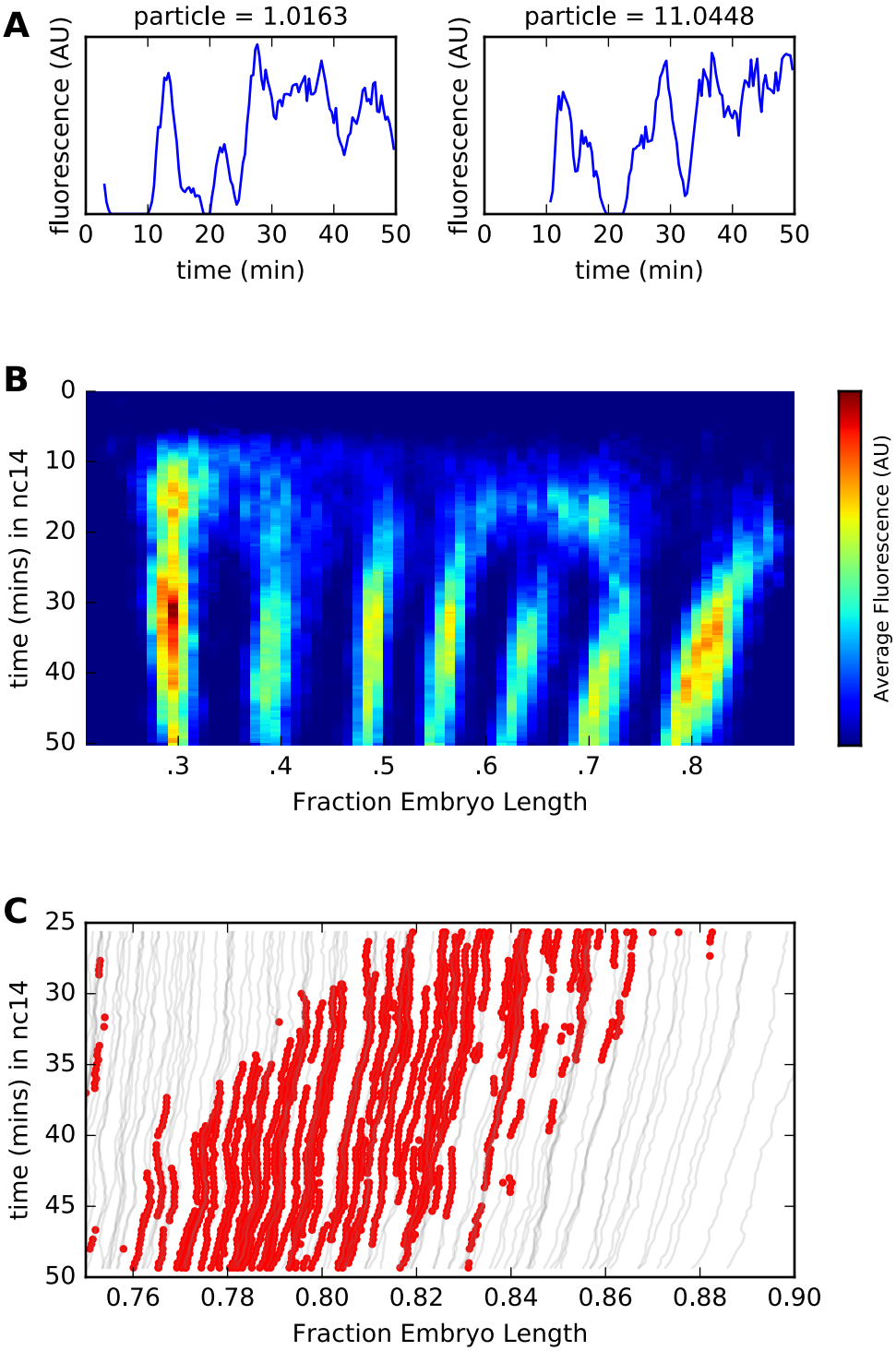

Figure 3. Spatiotemporal dynamics of *eve* expression

A) Fluorescence traces from three representative nuclei. B) Average fluorescence over space and time showing stripe formation, modulation and movement. The time resolution along the y-axis is 20s. The positions of nuclei along the x-axis were registered across movies based on the inferred position of stripe centers, and placed into bins of one percent embryo length, with the average fluorescence of all nuclei in each bin plotted. C) Traces of nuclei positions over time (gray lines) from stripe 7 region of movie EVE_D6 with timepoints where fluorescence is greater than 50,000 AU (the expected output for a promoter in the ON state for one 20s time interval) to illustrate stripe movement relative to nuclei.

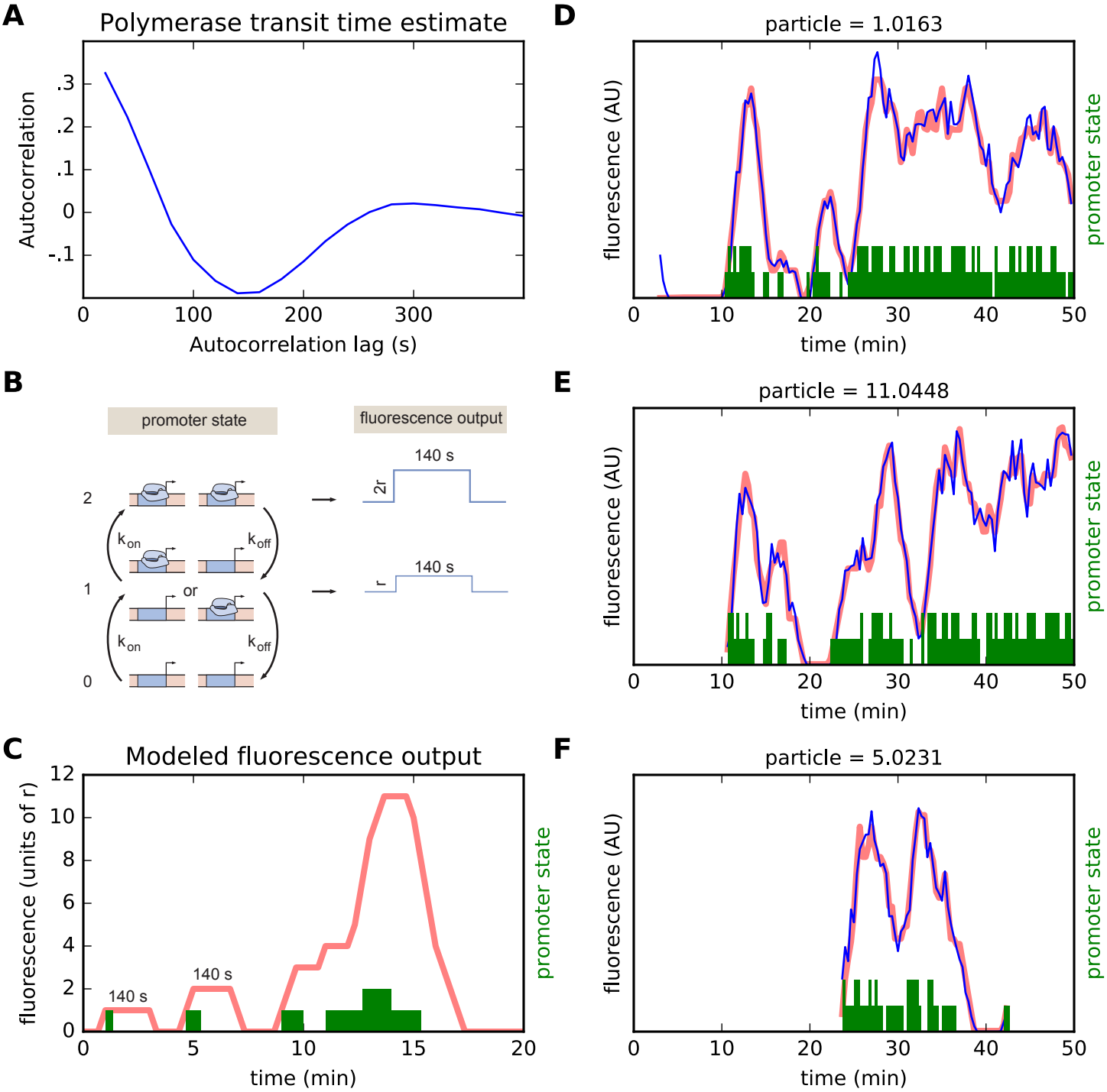

Figure 4. Modeling bursting in individual nuclei.

A) A key parameter in relating fluorescence output to the bursting state of a promoter is the time it takes for a polymerase to transit the gene, which we determined as approximately 140s by examining the autocorrelation of first derivative of measured fluorescence output. We expect this function to be at a minimum at the elongation time as polymerases added at time t leading to an increase in fluorescence will exit at time t + the elongation time leading to a matched decrease in fluorescence. B) Three state model accounting for post-replication presence of sister chromatids. When either promoter is on it loads polymerases at a constant rate contributing a pulse of polymerase that persists for 140s. C) Simplified example of the expected observed fluorescence (red line) produced from a hypothetic promoter state sequences. The fluorescence is the sum of the fluorescence pulses produced when one or both promoters are ON (green bars). D-F) Representative fluorescence traces from individual nuclei (blue lines), inferred bursting pattern (green bar means the promoter is ON; height represented number of engaged promoters) and fluorescence imputed by mHMM (red line).

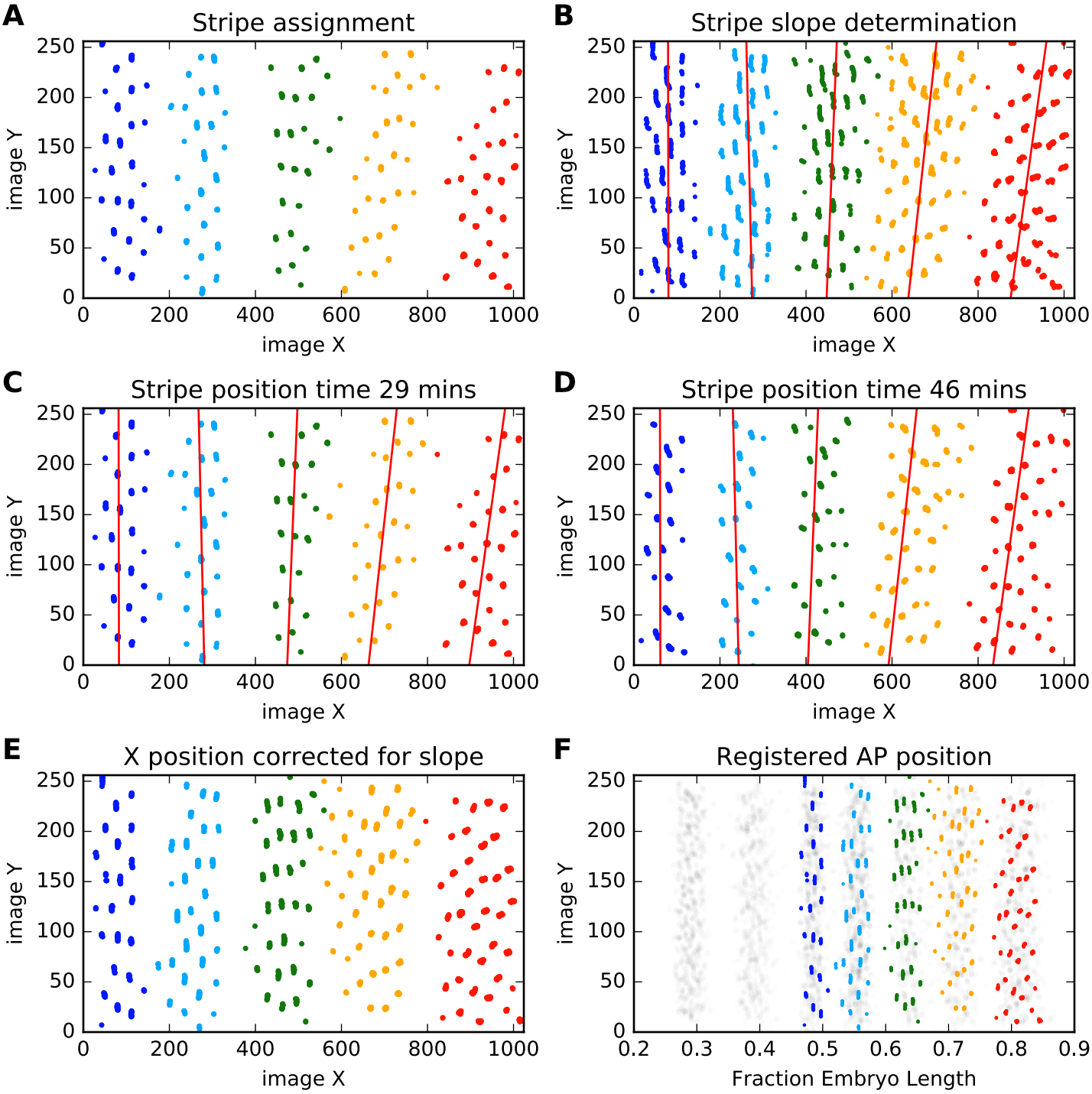

Figure 5. Stripe assignment and alignment

A) We preliminarily assign bursting nuclei to stripes by applying a Gaussian mixture model to each movie independently in overlapping six minute time windows with number of components equal to the number of stripes captured in that movie. An example is shown here from Movie 2. We next determine the orientation of each stripe to the imaging axes by fitting a line to coordinates of all nuclei from t > 25 mins assigned to that stripe in each movie, see panel B). We fit a line with this slope to bursting nuclei from each time window, examples of which are shown in (C) and (D). We use these fits to generate a linear model of the position of each stripe in each image over time, which we use to reorient the stripe so that it is perpendicular to the image x axis (E). Finally, we use the known coordinates of the anterior and posterior poles of the embryo to convert the image x axis to AP position, and register the stripes from different movies to each other. F) shows this final alignment with nuclei from Movie 2 colored by stripe and all other nuclei drawn in grey.

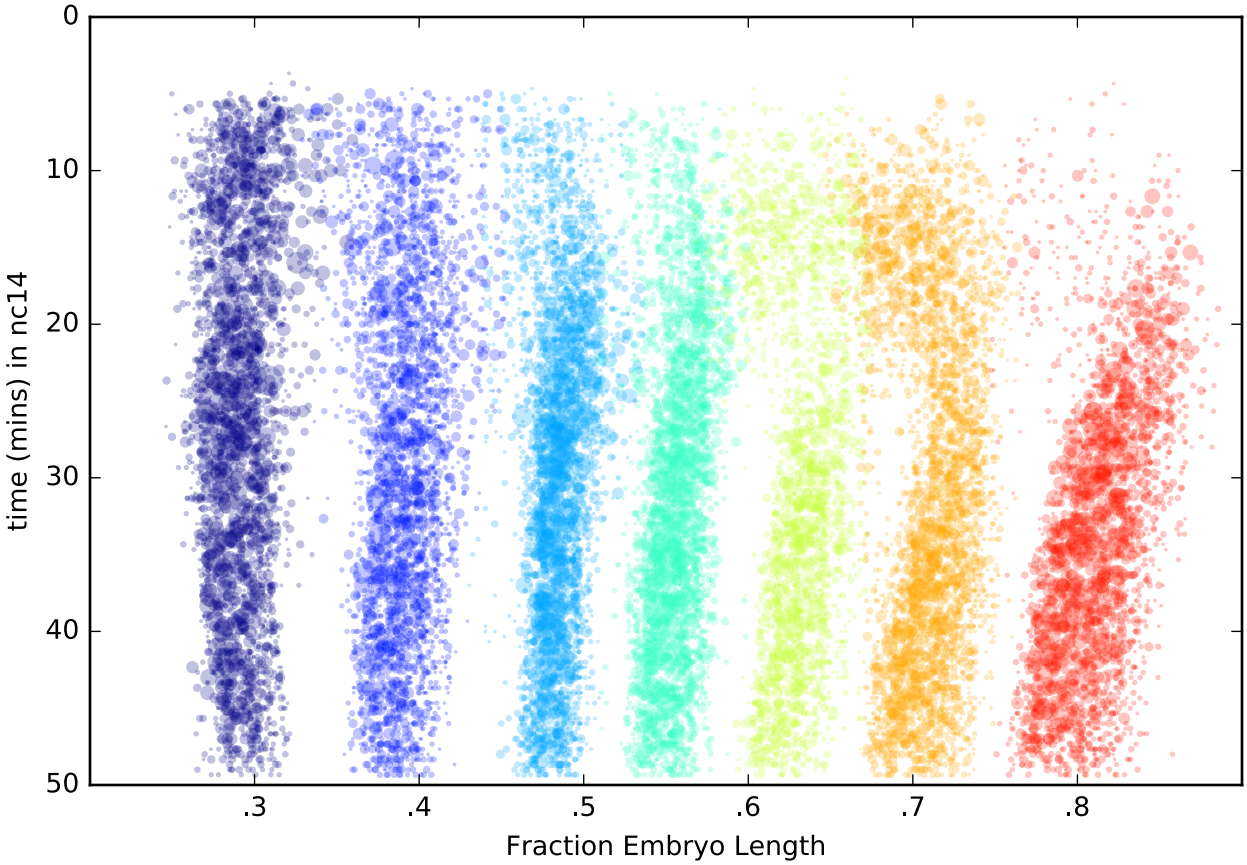

Figure 6. The kinetic fingerprint of *even-skipped* stripe formation

We inferred the location of every transcriptional burst in all 11 movies and plot here when (y-axis) and where along the anterio-posterior axis (plotted as fraction of embryo length) each burst occured. The size of the dot represents the duration of the burst. Collectively the data create a kinetic fingerprint of *eve* stripe formation.

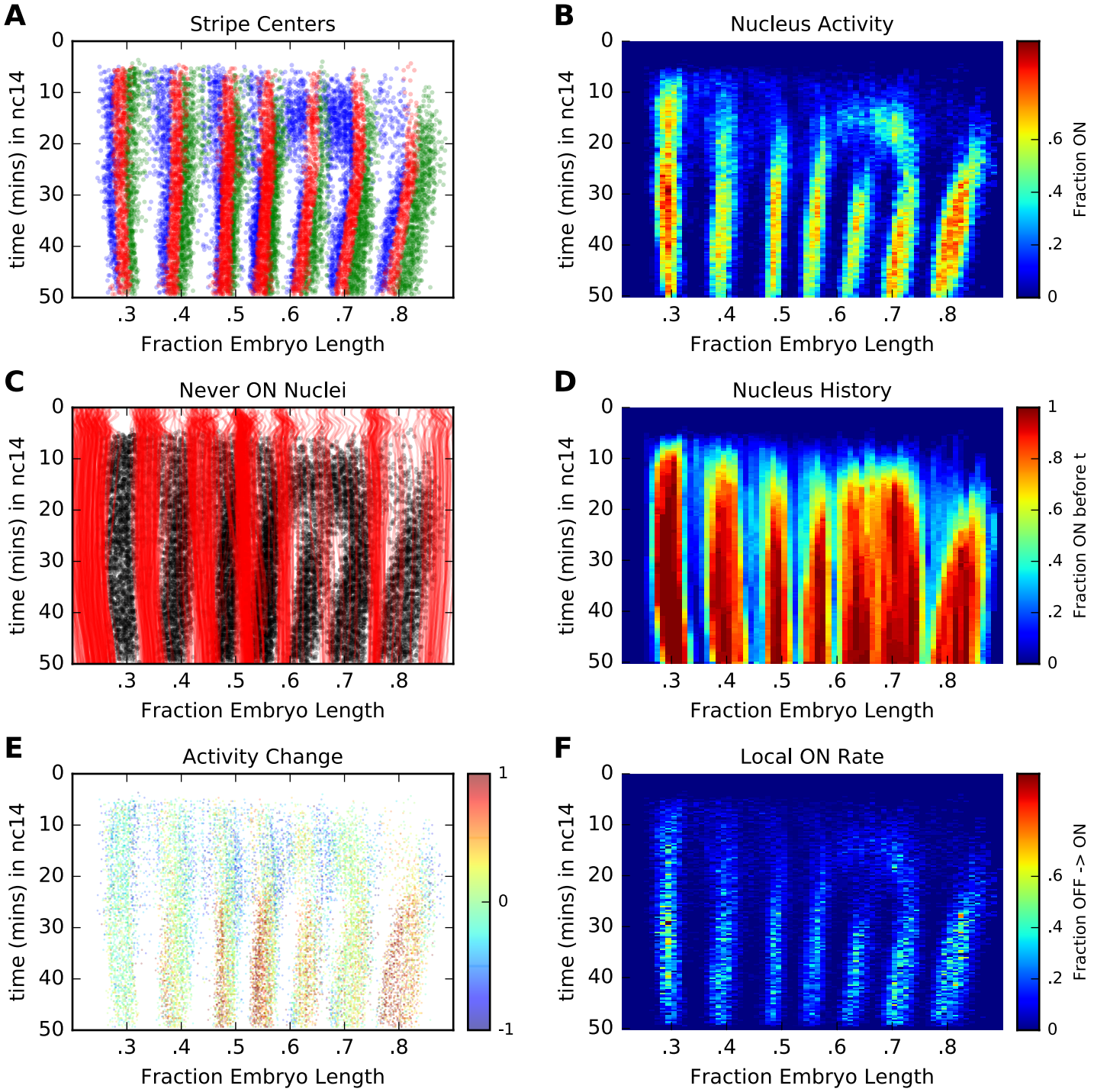

Figure 7. Stripes are formed from transcriptional deserts

A) Inferred positions of stripes (red) and stripe margins (ant. blue, post. green). Only locations of new transcriptional bursts are plotted. B) Mean activity (fraction of nuclei in an active state) over space and time. C) Locations of new bursts (black dots) in space and time along with spatiotemporal traces of nuclei that are in the OFF state throughout nc14 (red lines). D) Fraction of nuclei that have been on prior to given time (y-axis). E) Locations of new bursts colored by the change in activity of that nucleus from 0-25 minutes to 25-50 minutes into nc14. F) Local OFF to ON switching probability, computed by dividing the number of new bursts initiated in a given bin by the number of nuclei in OFF state.

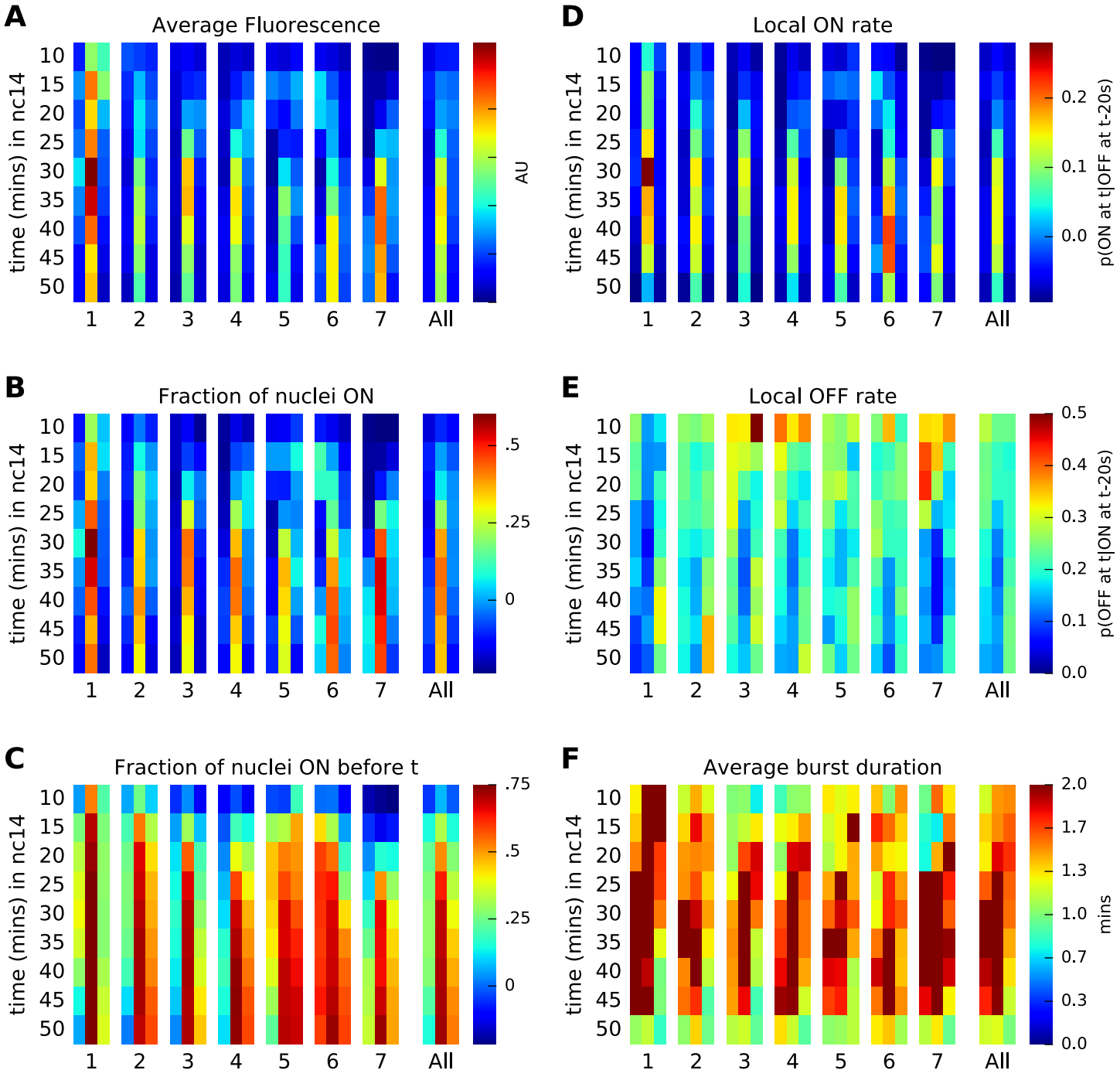

Figure 8. Variation in bursting parameters across time in stripes and stripe boundaries

Individual time points were binned based on stripe assignment and time (5 minute bins) and then various values were computed on these nuclei to highlight changes inside and outside of stripes over time. In each subpanel the left column is nuclei in the anterior flank of the stripe, the central column are stripe nuclei, and the right column are nuclei in the posterior flank. A) Average fluorescence. B) Activity (fraction of nuclei in ON state). C) Prior activity (fraction of nuclei that have been ON given time point or earlier). D) Local OFF to ON rate (fraction of nuclei in OFF state that switch to ON state). E) Local ON to OFF rate (fraction of nuclei in ON state that switch to OFF state). F) Average burst duration

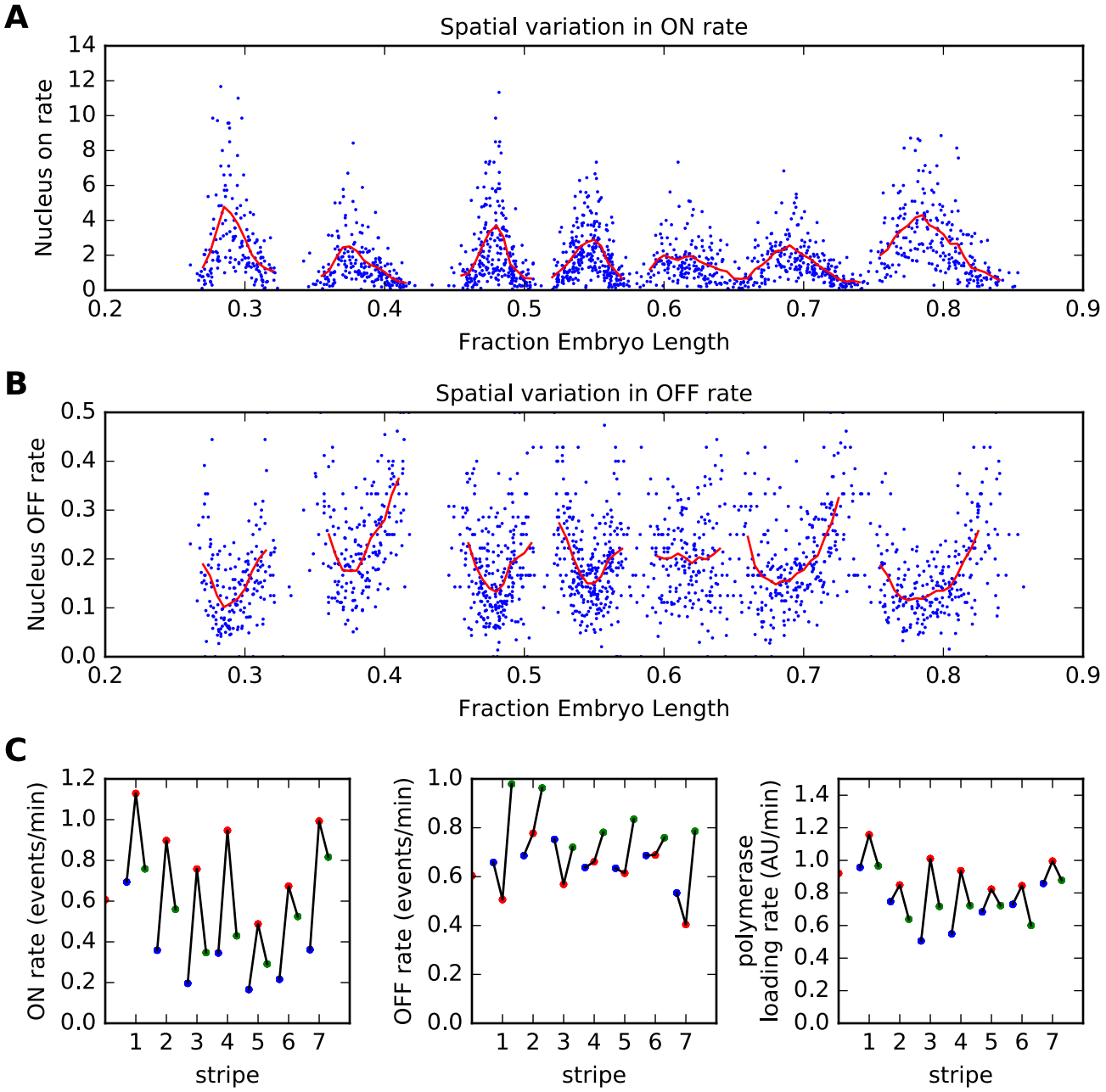

Figure 9. Variation in bursting parameters across stripe

A) Nucleus-specific ON rate for all nuclei (blue dots;). ON rate is number of OFF->ON transitions from mins 25-50 divided by number of time points in OFF state between first and last ON time point. Red lines are running averages in windows of .005 fraction of AP; breaks are points with fewer than 10 active nuclei. B) Nucleus-specific OFF rate for all nuclei (blue dots;). OFF rate is number of ON->OFF transitions from mins 25-50 divided by number of time points in ON state between first and last ON time point. Red lines are running averages in windows of .005 fraction of AP; breaks are points with fewer than 10 active nuclei. C) Stripe specific mHMM parameter inferences. Each triplet of points represents one stripe with the values for the posterior flank, stripe center, and anterior flank shown in blue, red and green.

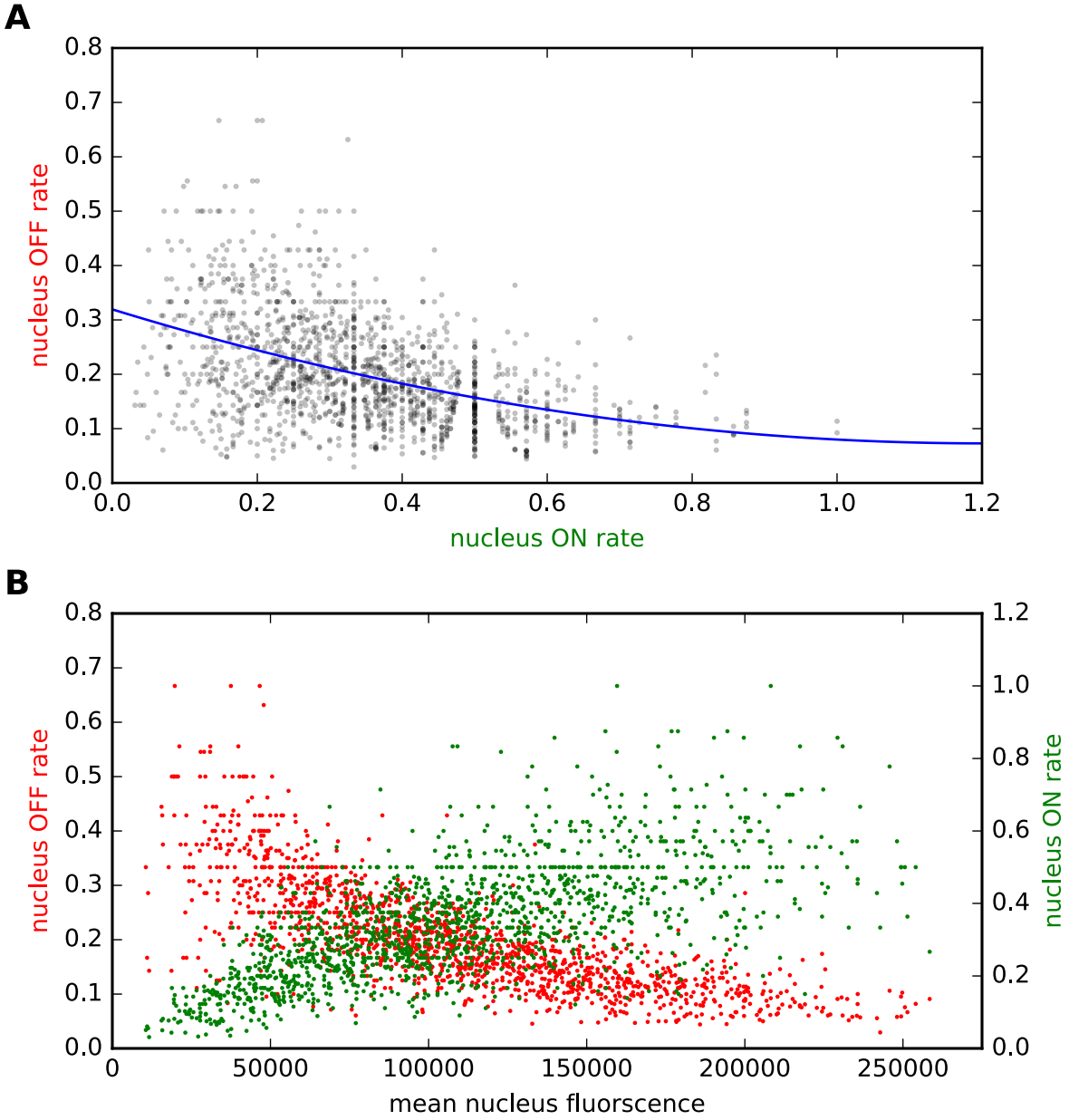

Figure 10. Anticorrelation of ON and OFF rates

We calculated empirical mean fluorescence, on rate (number of OFF to ON events divided by number of time points in OFF state) and off rate (number of ON to OFF events divided by number of time points in ON state) for all nuclei with at least one new burst between 25 and 50 mins in nc14. Only the period between active bursts was considered. For most nuclei this is the entire period from 25 mins through the end of their last burst. However for nuclei at stripe borders or in interstripe regions this is only a the non-quiescent portion of this time interval. We then compared these empircal ON and OFF rates to each other on a nucleus-by-nucleus level (A) or each individual to fluorescence (B), revealing high levels of correlation between these paramters.

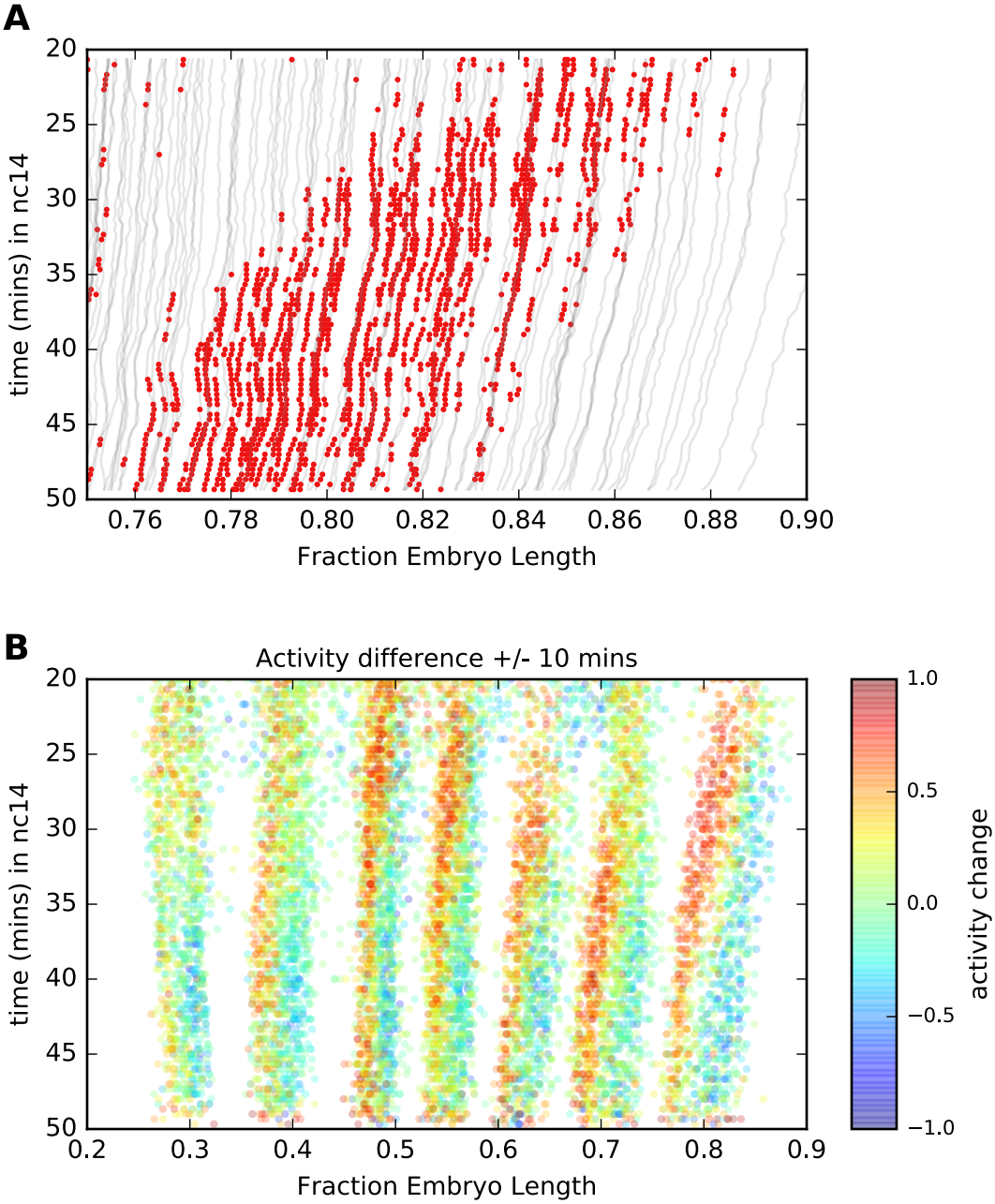

Figure 11. Stripe movement is driven by changes in nucleus state

A) Traces of nuclei positions over time (gray lines) from stripe 7 region of movie EVE_D6 with timepoints where new bursts initiated colored red to illustrate stripe movement relative to nuclei. B) Location of new bursts in space and time colored by the difference in their mean activity (fraction of timepoints in on state) in 10m after and 10m before the burst. Positive values represent a nucleus turning on or increasing activity, while blue values indicate a nucleus turning off or decreasing activity.

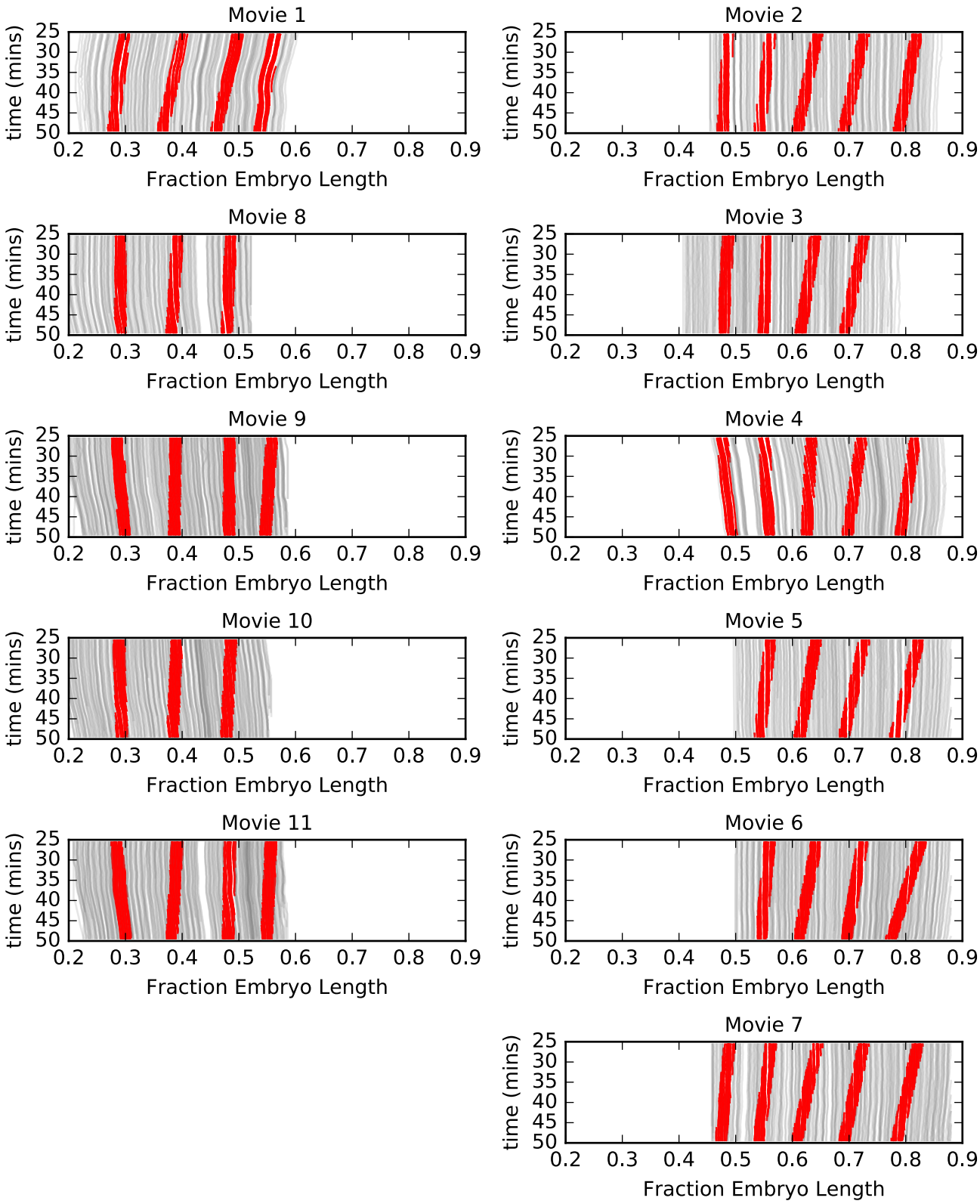

Figure 11-S1. Stripe movement

Traces of nuclei positions over time (gray lines) from all eleven movies with time points annotated as in stripes colored red.